Geoscientific
Model Development
Discussions

Development of an inorganic and organic aerosol model (Chimere2017β v1.0): seasonal and spatial evaluation over Europe

Florian Couvidat[1], Bertrand Bessagnet[1], Marta Garcia-Vivanco[2], Elsa Real[1], Laurent Menut[3], and Augustin Colette[1]

[1]Institut National de l'Environnement Industriel et des Risques, Verneuil-en-Halatte, France
[2]Centro de Investigaciones Energéticas, Medioambientales y Tecnológicas (CIEMAT), Departamento de Medio Ambiente, Av. Complutense 22, 28040-Madrid, Spain
[3]Laboratoire de Métérologie Dynamique, IPSL, CNRS, UMR8539, 91128 Palaiseau Cedex, France

Correspondence to: Florian Couvidat
(Florian.Couvidat@ineris.fr)

Abstract.

A new aerosol module was developed and integrated in the air quality model CHIMERE. Developments include an update of biogenic emissions and of the inorganic thermodynamic model ISORROPIA, revision of wet deposition processes and of the algorithms of condensation/evaporation and coagulation and the implementation of the SOA mechanism H^{2}O and the thermodynamic model SOAP.

Concentrations of particles over Europe were simulated by the model for the year 2013. Model concentrations were compared to the EMEP program observations and other observations available in the EBAS database to evaluate the performances of the model. Performances were determined for several components of particles (sea salts, sulfate, ammonium, nitrate, organic aerosol) with a seasonal and regional analysis of results.

The model gives good performances in general. For sea salts, the model succeeds in reproducing the seasonal evolution of concentrations for Western and Central Europe. For sulfate, except for an overestimation of sulfate in Northern Europe, modeled concentrations are close to observations with a good seasonal evolution of concentrations. For organic aerosol, the model performs well for stations with strong modeled biogenic SOA concentrations.

However, the model strongly overestimates ammonium nitrate concentrations during late autumn (possibly due to problems in the temporal evolution of emissions) and strongly underestimates SOA concentrations over most of stations (especially in the Northern half of Europe). This underestimation could be due to a lack of anthropogenic SOA in the model.

A list of recommended tests and developments to improve the model is also given.

1 Introduction

Atmospheric Particulate Matter (PM) contributes to adverse effects on health and ecosystems. The development of models is necessary to predict the formation of particles in order to evaluate their concentrations and to evaluate mitigation strategies. However, developing models with enough precision is quite challenging due to the complexity and variety of phenomena and

the great number of chemical species involved. Numerous air quality models have been developed to simulate PM concentrations (Emmons et al., 2010; Pozzoli et al., 2011; Zhang et al., 2010; Vestreng, 2003; Carlton et al., 2010; Menut et al., 2013; Sartelet et al., 2007).

PM is constituted of various chemical species: organic matter (OM), elemental carbon (EC) mainly originating from an-
5   thropogenic sources, major inorganic components (ammonium, nitrate and sulfate), sea salt, mineral dust and other crustal compounds. These species originate from numerous emission sources which can be natural (biogenic emissions from vegetation, sea-salt emissions, dust emissions) or anthropogenic (for example emissions from residential biomass burning, road traffic, agriculture, industrial sources). Particles can be primarily emitted in the atmosphere or secondary formed from chemical reactions.

10 OM typically represents between 20 and 60% (Kanakidou et al., 2005; Yu et al., 2007; Zhang et al., 2007) of the fine particulate mass and is formed via the partitioning of Semi-Volatile Organic Compounds (SVOC) between the gas and particle phases. These SVOCs can be primary in origin but OM is often considered to be mainly constituted of secondary organic compounds formed via the oxidation in the atmosphere of Volatile Organic Compounds (VOC) which can be biogenic (like isoprene, monoterpenes and sesquiterpenes) or anthropogenic (for example long-chain alkanes, toluene and other aromatics).
15 The oxidation (in the gas phase or in the aqueous phase) of sulfur dioxide SO_2 produces sulfuric acid H_2SO_4 which leads to sulfate formation via condensation or nucleation processes. If ammonia NH_3 is present in the atmosphere, it will neutralize sulfate and form ammonium. If there is still NH_3 available in the gas phase, it can lead to the formation of ammonium nitrate in the presence of nitric acid HNO_3 (formed via the oxidation of nitrogen oxides NO_x). Sea salts and natural dusts are primary natural particles and can interact with atmospheric pollutants. For example, HNO_3 can condense onto sea salts and leads to
20 sodium nitrate and then to the volatilization of chloride acid (HCl). Similarly, HNO_3 can condense onto dust and leads to the formation of calcium nitrate. As dust and sea salts are mainly coarse particles, these two processes can lead to the formation of coarse nitrate whereas ammonium nitrate will mainly remain in fine particles.

To simulate PM concentrations, models have to take into account the microphysics of particles (condensation/evaporation, coagulation, nucleation), chemical mechanisms for the gas-phase chemistry, aerosols thermodynamics, emissions and deposi-
25 tion processes. In the scope of this study, a new aerosol module has been developed in a modified version of the CHIMERE model. These modifications include an update of biogenic emissions and microphysics parameterizations, the implementation of thermodynamics model ISORROPIA v2.1 (Fountoukis and Nenes, 2007) and SOAP (Couvidat and Sartelet, 2015), the SOA mechanism of Couvidat et al. (2012) and modifications of deposition parameterizations. The results of the model were evaluated by comparison to measurements of $PM_{2.5}$ and PM_{10} concentrations but also of composition (Cl, Na, SO_4, NO_3, NH_4,
30 organic carbon).

The representation of several processes was revised to improve the results of the model:

– Biogenic emissions are computed with the MEGAN 2.1 algorithm (Guenther et al., 2012) with updated emission factors and Leaf Area Index (LAI) data.

Geoscientific
Model Development
Discussions

 - Below-cloud scavenging is represented as in Henzing et al. (2006) with a polydispersed distribution of cloud droplets (providing a distribution of droplet diameter as a function of rainfall). In-cloud scavenging is represented with the algorithm of Croft et al. (2010).

 - Evaporation/condensation of semi-volatile species is represented with the algorithm of Pandis et al. (1993) using thermodynamic equilibria. Coagulation of particles is represented as in Debry et al. (2007). Thermodynamic equilibria are computed with the ISORROPIA II model (Fountoukis and Nenes, 2007) for inorganic compounds and with the Secondary Organic Aerosol Processor SOAP (Couvidat and Sartelet, 2015) for organic compounds. The CHIMERE 2013 version used an older version of ISORROPIA 2.1 and a model for organic aerosol based on Pun et al. (2002).

 - The SOA formation mechanism of Couvidat et al. (2012) is used for toluene, xylene and biogenic VOC. The CHIMERE 2013 version used the mechanism of Bessagnet et al. (2008).

 - The amount of water in particles is calculated as a function of humidity and the composition of particles using ISORROPIA. This amount is used to calculate the wet density of particles (with water) and the wet diameter of particles which are used to compute the kinetics of absorption, coagulation and deposition instead of the dry values as in Menut et al. (2013).

The aerosol module is described in the part of the paper. The second part focuses on the comparison of modeled concentrations with observations for Cl, Na, SO_4, NO_3, NH_4, organic carbon, $PM_{2.5}$ and PM_{10} with a regional and seasonal analyses of results.

2 Method

The CHIMERE 2013 version (Menut et al., 2013) was modified to update some parameterizations and chemical mechanisms. The modified version of CHIMERE was then evaluated for the simulation of PM concentration and composition over Europe in 2013.

2.1 Model development

2.1.1 Chemical mechanisms

A simple aqueous-phase chemical mechanism is used for sulfate formation from the oxidation of SO_2 in clouds. This mechanism assumes that the aqueous-phase concentrations of SO_2, H_2O_2 and O_3 are at equilibrium with the gas phase with a partitioning being function of pH for SO_2. The pH of clouds is computed by taking into account the absorption and dissociation of various acids (H_2SO_4, HCl, HNO_3 and H_2CO_3) and the formation of NH_4^+. The electroneutrality equation is solved with the Newton-Raphson method. Henry's law constants, equilibrium constants are taken from Seinfeld and Pandis (1998).

For SVOC formation that leads to the formation of SOA compounds after partitioning, the mechanism of Couvidat et al. (2012) is used. The mechanism is shown in Table 1. It takes into account the formation of SVOC from biogenic (isoprene,

monoterpenes, sesquiterpenes) and anthropogenic precursors (toluene, xylenes) under high-NO_x and low-NO_x conditions.

In Couvidat et al. (2012), Primary Organic Aerosols (POA) are assumed to be SVOC and are split into three compounds POAlP, POAmP and POAhP (having respectively a low, medium and high volatility) to follow the dilution curve of POA in Robinson et al. (2007). The aging of these compounds is also taken into account with a reaction with OH which leads to less volatile compounds SOAlP, SOAmP and SOAhP via the following reactions:

$$POAlP + OH \xrightarrow{k} SOAlP \tag{1}$$

$$POAmP + OH \xrightarrow{k} SOAmP \tag{2}$$

$$POAhP + OH \xrightarrow{k} SOAhP \tag{3}$$

with k the kinetic rate constant equal to 2×10^{-11} molecules^{-1}.cm^3.s^{-1}. Following Grieshop et al. (2009), aging was assumed to lead to a decrease of volatility by a factor 100 (SOAlP, SOAmP and SOAhP are respectively less volatile by a factor 100 than POAlP, POAmP and POAhP).

2.1.2 Biogenic emissions

Biogenic emissions are computed with the Model of Emissions and Gases and Aerosols from Nature MEGAN 2.1 algorithm (Guenther et al., 2012), which was implemented in CHIMERE. It uses meteorological conditions (Temperature, Solar radiation and soil moisture), the Leaf Area Index and the Plant Functional Type (PFT) to compute biogenic emissions. In this study, the above-canopy model is used. The effect of soil moisture on isoprene emissions is not taken into account because of no Wilting Point (i.e. the soil moisture level below which plants cannot extract water from soil) database are available over Europe. Therefore, isoprene emissions may be overestimated during dry periods.

High spatiotemporal data (30 arc-seconds every 8 days) generated from MODIS (Yuan et al., 2011) were used for LAI inputs. The 30 arc-seconds USGS (US Geophysical Survey) landuse database was used to provide information on the plant functional type. The PFT was then combined with the emissions factors for each functional type of Guenther et al. (2012) to compute the landscape average emissions factors.

2.1.3 Anthropogenic emissions

VOC emissions are used as in Menut et al. (2013) except for primary SVOC emissions, a SVOC/POA factor is applied to convert POA emissions into SVOC emissions. In Couvidat et al. (2012), a SVOC/POA factor of 5 was used on the basis that SVOC primary emissions were underestimated. With this factor, the model was able to simulate the strong concentrations of

organic aerosols in winter and to give satisfactory results over most of Europe. Denier van der Gon et al. (2015) has shown that POA emissions are greatly underestimated due to a strong underestimation of residential wood burning emissions by a factor 3 over Europe (between 1 and 10 depending on the countries) if SVOC emissions are included. By correcting POA emissions and assuming that Intermediate-Volatility Organic Compounds (IVOC) are missing from the inventory (with the assumption

5   that IVOC emissions are equal to 1.5 POA emissions), the authors obtained satisfactory results in winter but still with an underestimation of OM from biomass burning. The authors used therefore a total (IVOC+SVOC)/POA factor of 7.5.

In this study, a SVOC/POA of 5 is used for residential emissions (without adding IVOC emissions) and 1 for other sectors (assuming therefore that no SVOC emissions from other sectors are missing). However, IVOCs are not taken into account because of the large uncertainties on their emissions and their oxidation mechanism. Pye and Seinfeld (2010) used naphthalene

10   as a surrogate for IVOC and used the yields from smog chamber experiments (Chan et al., 2009; Kautzman et al., 2010) to develop a mechanism of IVOC oxidation. The authors found that only minor concentrations of SOA are formed from IVOC (only 5% of total OM) whereas Zhao et al. (2016a) simulated strong concentrations of SOA from IVOC contributing to half the OA over China. However, Pye and Seinfeld (2010) argued that naphthalene may not be an appropriate choice for the surrogate species. Platt et al. (2013) investigated the SOA formation from gasoline vehicle in an environmental reaction chamber and

15   found that only a small part of SOA could be explained by the oxidation of aromatics compounds and therefore most of the SOA formation could be attributed to the oxidation of IVOC. This result is however contradicted by Nordin et al. (2013) who found that most of the SOA formation is due to the oxidation of aromatics compounds.

2.1.4   Thermodynamic of Secondary organic and inorganic aerosol

20   Two thermodynamic modules were implemented inside CHIMERE to take into account the formation of secondary aerosols: ISORROPIA v2.1 (Fountoukis and Nenes, 2007) for inorganic aerosols and the Secondary Organic Aerosol Processor (SOAP) (Couvidat and Sartelet, 2015) for organic aerosols. Due to the lack of information on the dust composition, crustal elements are not taken into account for the partitioning whereas it can strongly impact the formation of ammonium nitrate (Ansari and Pandis, 1999; Moya et al., 2002). However, a simple reaction (described in section "Condensation/evaporation") is added to

25   CHIMERE to take into account the formation of calcium nitrate as done by Hodzic et al. (2006).

SOAP computes the partitioning of organic compounds between the gas and particle phases according to the complexity required by the user. It uses the molecular surrogate approach in which surrogate compounds are associated with molecular structures to estimate several properties and parameters (hygroscopicity, absorption into the aqueous phase of particles, activity coefficients and phase separation). Each surrogate can be hydrophilic (condenses only into the aqueous phase of particles), hy-

30   drophobic (condenses only into the organic phases of particles) or both. Activity coefficients are computed with the UNIFAC (UNIversal Functional group Activity Coefficient; Fredenslund et al. (1975)) thermodynamic model for short-range interactions and with the Aerosol Inorganic-Organic Mixtures Functional groups Activity Coefficients (AIOMFAC) parameterization for medium- and long-range interactions between electrolytes and organic compounds (Zuend et al., 2008, 2011; Zuend and Seinfeld, 2012; Ganbavale et al., 2015).

SOAP can simulate SOA formation with either an equilibrium representation or a dynamic representation of organic aerosol condensation processes. The dynamic representation takes into account the condensation/evaporation kinetic of organic compounds and their diffusion in the particle by dividing the organic particle into several layers. However, this method requires a lot of computing time. Therefore, in a first approach, the equilibrium approach of SOAP is used.

As in Couvidat et al. (2012), SOA surrogate compounds are assumed to be either hydrophilic or hydrophobic and the impact of medium-range and long-range interactions on activity coefficients are not taken into account. For hydrophilic acids, SOAP takes into accounts for the dissociation of organic acids at high pH as a function of their dissociation constant. Moreover, Pun and Seigneur (2007) developed a parameterization to take into account the impact of pH on the oligomerization of aldehyde compounds by computing an effective Henry's law constant:

$$H_{eff} = H \left(1 + 0.1 \left(\frac{a(H^+)}{10^{-6}} \right)^{1.91} \right) \tag{4}$$

where H_{eff} is the effective Henry's law constant of BiA0D (surrogate species of the H^2O mechanism for aldehydes formed from the oxidation of monoterpenes), H is the monomer Henry's law constant of BiA0D, and $a(H^+)$ is the activity of protons in the aqueous phase.

Thermodynamic properties of biogenic and anthropogenic species are shown in Tables 2. Table 3 shows the properties of primary SVOC compounds (POAlP, POAmP, POAhP) and their aging products.

2.1.5 Computation of the wet diameter and the wet density of particles

Several parameterizations (condensation/evaporation, coagulation, particle deposition) depend on the particle diameter $D_{p,wet}$ which is different from the dry diameter (without water) $D_{p,dry}$. Similarly, dry deposition of particles depends on the wet density d_w of particles.

To compute the wet diameter $D_{p,wet}$ and the wet density d_w, ISORROPIA is used to compute the amount of water absorbed by each size bin as a function of the composition and the relative humidity. The method of Semmler et al. (2006) is used to compute the density of the liquid aqueous phase d_l. The volume of the whole particle is computed with:

$$V_{tot} = V_{solid} + V_{liq,inorg} + V_{org} \tag{5}$$

With V_{tot} the volume of the whole particle, V_{solid} the volume of the solid part of the particle (including dust, black carbon), $V_{liq,inorg}$ the volume of the aqueous phase (including Na, Cl, SO_4, NH_4, NO_3 and H_2O) and V_{org} the volume of the organic phase of particles. For simplification purposes, the organic phase density is assumed to be equal to 1300 kg/m^3 and the density of the aqueous phase is assumed to be not influenced by hydrophilic organic compounds.

Using the density of the solid phase d_{sol} (assumed to be equal to 2200 kg/m^3), the density of the liquid aqueous phase d_l and the density of the organic phase d_{org}, Eq. 5 leads to:

$$d_w = \left(\frac{w_{solid}}{d_{solid}} + \frac{w_{liq,inorg}}{d_l} + \frac{w_{org}}{d_{org}} \right)^{-1} \tag{6}$$

Geoscientific
Model Development
Discussions

With w_{solid}, $w_{liq,inorg}$ and w_{org} the mass fraction of respectively the solid phase, the aqueous phase and the organic phase. The wet diameter can be computed with the following equation given by the ratio of the volume of the wet particle to the volume of the dry particle:

$$\frac{D_{p,wet}^3}{D_{p,dry}^3} = \frac{1}{1 - w_{H_2O}} \frac{d_{dry}}{d_{wet}} \tag{7}$$

with w_{H_2O} the mass fraction of water in the particle and d_{dry} the dry density of the particle which can be computed with Semmler et al. (2006) and Eq. 5 without taking into account the mass of water.

2.1.6 Dry deposition of particles and semi-volatile organic species

Dry deposition is parameterized via a downward flux $F_{dry,i}$ such as:

$$F_{d,i} = -v_{d,i} * C_i \tag{8}$$

with v_d the deposition velocity. The deposition velocity is represented via the resistance analogy of Wesely (1989). For each gaseous species i, $v_{d,i}$ is calculated with:

$$v_{d,i} = \frac{1}{R_a + R_{b,i} + R_{c,i}} \tag{9}$$

with R_a the aerodynamic resistance associated with turbulent transport in the atmosphere, $R_{b,i}$ the quasi-laminar resistance and $R_{c,i}$ the surface resistance.

The surface resistance depends on the nature of the surface and is generally divided into three categories: water, ground and vegetation. For the deposition of gases to water and vegetation, the parameterizations depend on the Henry's law constants of compounds i. For O_3, SO_2, NO_2, NO and NH3, the values of Menut et al. (2013) are used.

For SVOC, Bessagnet et al. (2010) showed that without dry deposition of gas-phase SVOC could lead to an overestimation of SOA by 50 %. As done by Bessagnet et al. (2010), Henry's law constants of SVOC are used to take into account their deposition. The Henry's law constants of hydrophilic species are taken from Couvidat et al. (2012). For hydrophobic species, they were calculated using the activity coefficients at infinite dilution as in Couvidat and Seigneur (2011), by using the saturation vapour pressure P^0 and the activity coefficient of compound i at infinite dilution computed with UNIFAC γ_i^∞ such as:

$$H_i = \lim_{C_i \to 0} \left(\frac{C_i}{P_i} \right) = \frac{\rho_{eau}}{M_{eau} \times \gamma_i^\infty \times P_i^0} \tag{10}$$

with ρ the density of water. For primary SVOC (POAlP, POAmP and POAhP), a Henry's law constant of 0.01 mol/L/atm is used (similar to the Henr's law constant of alkanes). For their aging products, a Henry's law constant of 3000 mol/L/atm is used (for a slightly oxidized molecule). Table 4 shows the Henry's law constants used in this study.

For dry deposition of particles, the parameterizations of Menut et al. (2013) are used. However, the wet diameter and the wet density are used instead of the dry values.

2.1.7 Wet deposition of particles and semi-volatile species

In-cloud scavenging for both gases and aerosols is represented by the parameterization of Croft et al. (2010), assuming that wet deposition by in-cloud scavenging is proportional to the amount of cloud water lost by precipitations, such as:

$$\frac{dC}{dt}_{incl} = \frac{\zeta_l f_l p_r}{w_l h} C \tag{11}$$

with p_r the precipitation rate (in $g\,cm^{-2}\,s^{-1}$), w_l the liquid water content of clouds (in $g\,cm^{-3}$), C the concentration and h the height of the cell (in cm) f_l is the fraction of the compound present in the cloud and ζ_l an empirical uptake coefficient chosen equal to 1.

For gases, f_l is computed with the effective Henry's law constant and the liquid water content. For particles, f_l is taken as 1 except for particles with a diameter lower than a dry critical radius (chosen equal to 0.1 μm) which are assumed to be too small to form clouds due to the Kelvin effect.

For the below-cloud scavenging of gases and particles, deposition is described by a scavenging coefficient λ (in s^{-1}) such as:

$$\frac{dC}{dt} = -\lambda C \tag{12}$$

For gases, the scavenging coefficient λ_g can be calculated with the following equation assuming an irreversible scavenging (Seinfeld and Pandis, 1998):

$$\lambda_g = \int_0^\infty 2\pi D_{dif} Sh R N(R) dR \tag{13}$$

with R the radius of the droplet colliding with the gas, D_{dif} the molecular diffusion coefficient of the deposited compound, Sh is the Sherwood number describing the transfer of gases from air towards a raindrop and N(R) is the number of rain droplets distribution function.

For particles, the scavenging coefficient is expressed by (Seinfeld and Pandis, 1998):

$$\lambda_g = \int_0^\infty \pi R^2 U_t E(R, R_p) N(R) dR \tag{14}$$

with U_t the terminal velocity of the droplet (in m/s) and $E(R, R_p)$ the collision efficiency between a droplet of radius R and a particle of radius R_p.

Following Henzing et al. (2006), the rain droplet velocity parameterization of Mätlzer (2002) and the rain droplet size distribution parameterizations of de Wolf (1999) are used:

$$U_t = 0 \qquad\qquad R < 0.015 mm \tag{15}$$

$$= 4.323(R - 0.015) \qquad\qquad 0.015 \leq R \leq 0.3 mm \tag{16}$$

$$= 9.65 - 10.3 exp(-0.3R) \qquad\qquad R > 0.3 mm \tag{17}$$

Geoscientific
Model Development
Discussions

$$N(R) = \left(1.047 - 0.0436 * ln(P) + 0.00734 * (lnP)^2\right) \times 1.98 \times 10^{-5} P^{-0.384} R^{2.93} exp\left(-5.38 P^{-0.186R}\right) \tag{18}$$

2.1.8 Condensation/evaporation

Absorption is described by the "bulk equilibrium" approach of Pandis et al. (1993). In this approach, all the bins for which condensation is very fast are merged into a "bulk particulate phase". Following Debry et al. (2007), a cutting diameter of 1.25 μm is used to separate bins which are inside the "bulk particle" (with a diameter lower than the cutting diameter). Thermodynamic models are used to compute the partitioning between the gas and particle phases and estimate the gas-phase concentrations at equilibrium. The equilibrium concentration G_{eq} is calculated by the thermodynamic module ISORROPIA for inorganic semi-volatile compounds and by SOAP for SVOC.

The mass of compounds condensing onto particles ΔA_p is redistributed over bins according to the kinetic of condensation into each bin whereas the mass of compounds evaporating from each bin is proportional to the amount of the compounds in the bins. If the variation of particulate bulk concentration of compound i $\Delta A_{p,i} > 0$:

$$\Delta A_{p,i}^{bin} = \frac{k^{bin}}{\sum_j k_i^j} DeltaA_{p,i} \tag{19}$$

with k_i^{bin} the kinetic of condensation given by Seinfeld and Pandis (1998):

$$k_i^{bin} = Number^{bin} \frac{2\pi D_{p,wet}^{bin} D_i M_i}{RT} f(Kn,\alpha) \tag{20}$$

with $Number^{bin}$ the number of particles inside the bin, D_p^{bin} the mean diameter of the bin, D_i the diffusion coefficient for species i in air, M_i its molecular weight and $f(Kn,\alpha)$ is the correction due to non-continuum effects and imperfect surface accommodation.

If the variation of particulate bulk concentration of compound i $\Delta A_{p,i} < 0$:

$$\Delta A_{p,i}^{bin} = \frac{A_{p,i}^{bin}}{\sum_j A_{p,i}^j} DeltaA_{p,i} \tag{21}$$

The absorption flux J ($\mu g m^{-3} s^{-1}$) of a semi-volatile inorganic or organic species onto a bin computed with:

$$J = \frac{1}{\tau} \Delta A_{p,i}^{bin} \tag{22}$$

with τ the time to reach equilibrium (chosen equal to the time step of integration).

The gas to particle conversion of HNO_3 onto dust and sea salts is also taken into account. HNO_3 can indeed react with calcite $CaCO_3$ of dusts to form calcium nitrate $Ca(NO_3)_2$. HNO_3 can also react with dolomite ($MgCa(CO_3)_2$) but only the reaction with calcite is taken into account. Formenti et al. (2008) found a mass fraction of Ca in dusts between 4% and 9%. A calcium fraction of 6% is used. In sea salts, HNO_3 can replace the Cl present in sea salt and leads to the volatilization of HCl. Both reactions were assumed to be limited by the condensation kinetic of HNO_3 onto particles as in Hodzic et al. (2006).

2.1.9 Coagulation

The flux of coagulation $J^{bin}_{coag,i}$ of a coumpound i inside a bin b is computed with the size binning method of Jacobson and Turco (1994):

$$J^b_{coag,i} = \sum_{j=1}^{b} \sum_{k=1}^{b} f^b_{j,k} K_{j,l} A^j_{p,i} Number^k - A^b_{p,i} \sum K_{bin,j} Number^k \qquad (23)$$

with $K_{j,l}$ the coagulation kernel coefficient between bins i and j and $f^b_{j,k}$ the partition coefficient (the fraction of the particle created from the coagulation of bins j and k which is redistributed inside bin b). The coagulation kernel and the partition coefficient are calculated as in Debry et al. (2007).

2.2 Simulation set-up

The new model was run to simulate the concentrations of particles and their composition in 2013 over Europe with a resolution of 0.25°x0.25°. Meteorology was obtained from Integrated Forecasting System (IFS) model of the European Centre for Medium-Range Weather Forecasts (ECMWF). The meteorology was evaluated in Bessagnet et al. (2016) for 2-meter Temperature, 10-meter Wind Speed and the Planetary Boundary Layer (PBL) for the model intercomparison project Eurodelta III. The authors reported high correlations for temperature (between 0.88 and 0.94) over the whole domain and a slight underestimation of Temperature (between -0.3K and -0.7K), an overestimation of the Wind Speed from 0.1 to 0.9 m/s and an underestimation of the PBL around -100 m (although ECMWF in the Eurodelta III project was shown to be one of model with the lowest RMSE). Anthropogenic emissions of gases and particles were taken from the EMEP inventory (Vestreng, 2003) and Boundary Conditions were generated from the Model for OZone And Related Tracers (Mozart v4.0 (Emmons et al., 2010)).

For PM$_{2.5}$, PM$_{10}$ and each component of PM, several statistics were computed: Root Mean Square Error (RMSE), the correlation coefficient, the Mean Fractional Error (MFE) and the Mean Fractional Bias (MFB). Boylan and Russell (2006) defined two criteria to estimate the performances of the model. The model performance criteria (described as the level of accuracy that is considered to be acceptable for modeling applications) is reached when MFE $\leq$ 75% and when MFB $\leq \pm$ 50% whereas the performance goal (described as the level of accuracy that is considered to be close to the best a model can be expected to achieve) is reached when MFE $\leq$ 50% and when MFB $\leq \pm$ 30%. Although these criteria are not recent, they provide a useful basis to evaluate models.

The seasonal evolution of statistics was examined to study the performances of the model for different seasons and to separate performances over a month from annual performances. The statistics were also computed by "regions" gathering countries having similar features. 5 regions were selected:

– Southern Europe gathering Spain, Portugal and Italy

– Western Europe gathering Ireland, Great Britain and France

- Central Europe gathering Germany, Belgium, Netherlands, Switzerland, Denmark and Austria

- Northern Europe gathering Norway, Sweden and Finland (characterized by low temperatures and low concentrations of particles)

- Eastern Europe gathering the other countries at the east of Europe

A map of regions and stations referred hereafter is shown in Figure 1.

2.3 Observations

Results of the model are compared to various measurements (NO_3, NH_4, SO_4, Na, Cl, OC, PM_1, $PM_{2.5}$ and PM_{10}) available in the EBAS database. EBAS is a database hosting observation data of atmospheric chemical composition and physical properties in support of a number of national and international programs ranging from monitoring activities to research projects. EBAS is developed and operated by the Norwegian Institute for Air Research (NILU). This database is mostly populated by the EMEP (European Monitoring and Evaluation Programme) measurements (Tørseth et al., 2012).

3 Results

3.1 Sea salts

Annual scores for sodium (Na) and chloride (Cl) are given in Table 5. Comparisons are carried out over 38 stations for Na and 35 stations for Cl. Scores are very similar between Na and Cl. The simulated mean concentrations are close (0.67 μg m^{-3} for Na and 1.28 μg m^{-3} for Cl) to the measured mean concentrations (0.69 μg m^{-3} for Na and 1.17 μg m^{-3} for Cl) and the spatiotemporal correlations are high (0.66 for Na and 0.67 for Cl). MFB are low (6% for Na and 9% for Cl) and MFE (52% for Na and 49% for Cl) are close to the goal criteria of Boylan and Russell (2006) (MFE $\leq$ 50% and MFB $\leq \pm$ 30%). Figure 2 shows the annual concentrations and MFB of Na and Cl at each station. Only one station in Spain underestimates (along the Bay of Biscay) concentrations for Na. Most stations in Spain, Central Europe and Western Europe have a low annual bias for Na whereas most stations in Northern and Eastern Europe seem to have a high MFB with overestimated concentrations. Results are similar for Cl except in Spain with overestimations observed near the Mediterranean Sea and in some stations in Central Europe far from the seas. This may indicate that the kinetic of HNO_3 condensation onto sea salts and the evaporation of HCl is not important enough.

Figure 3 shows the seasonal evolution of the statistics by regions. The same behavior was found for Cl concentrations than for Na concentrations.

Na concentrations seem to be underestimated for the stations in the Southern Europe (only stations in Spain for Na and Cl) from April to October with MFB reaching -60% and the MFE is between 60% to 80% throughout all the year. The temporal correlation is high but the spatial correlation is low. However, for the station ES0008R along the Bay of Biscay with strong observed of Na (with several peaks higher than 6 μg m^{-3}), the model underestimates the concentrations. It could then be possible

that Na concentrations at this station cannot be reproduced due to the low resolution of the model and the strong evolution of concentrations between the sea and the land. The other stations have all a similar pattern shown in Figure 3. Concentrations of Na are overestimated by the model in late Autumn and Winter (with a MFB from 30% to 60%) whereas concentrations are underestimated from June to October with a MFB of -60%. Measurements give higher concentrations of Na in summer and

5 lower concentrations in winter whereas the model simulate the opposite trend.

For the stations in Western Europe and Central Europe, the model gives satisfactory results and is able to reproduce the seasonal evolution of Na concentrations with MFE around 40 % and MFB between +20% and -20% except for February in Central Europe. Correlations are high (between 50% and 80% in Western Europe around 80% in Central Europe). RMSE are relatively low for Western Europe (between 0.6 and 1.1 μg m^{-3} for concentrations between 0.8 and 1.7 μg m^{-3}) whereas

10 RMSE for Central Europe are of the same range than measured and modeled concentrations (between 0.4 and 1.6 μg m^{-3}).

For Eastern and Northern Europe, the model overestimates concentrations throughout the year with MFB often higher than 50% for Eastern Europe and often higher than 30% for Northern Europe and with high MFE (often higher than 50% and even exceeding 100% for some months in Eastern Europe). However, if relative errors are high in Eastern Europe, absolute errors are low (RMSE lower than 0.35 μg m^{-3}) because concentrations in Eastern Europe are very low (mean concentrations lower

15 than 0.12 μg m^{-3} and modeled concentrations between 0.09 and 0.35 μg m^{-3}). This overestimation could be due to a lack of sea salts deposition in the model which becomes significant for low concentrations far from seas. Such an underestimation of deposition was reported in Tsyro et al. (2011); Neumann et al. (2016).

3.2 Sulfate

20 Annual scores for SO$_4$ are given in Table 5. Comparisons are carried out over 56 stations. The simulated mean concentrations (1.66 μg m^{-3}) and the measured mean concentrations (1.60 μg m^{-3}) are very close. The spatiotemporal correlation is high (0.67). MFB is low (13%) but indicates a slight relative overestimation. MFE is below 50% (44%) and therefore the goal criteria of Boylan and Russell (2006) is respected for sulfate. The RMSE is equal to 1.13 μg m^{-3}. Figure 4 shows the annual concentrations and MFB of SO$_4$ at each station. Most stations give satisfactory results, 41 stations have a MFB between $\pm$

25 30% and 33 stations respect the goal criteria. The model gives no stations where SO$_4$ concentrations would be significantly underestimated (MFB<-30%) but results at some stations are significantly overestimated, especially in the North of Europe. This overestimation is similar to the overestimation of sea salts in Northern Europe. However, the contribution of sulfate from sea salts in the model (7.68 %) is not enough to explain the overestimation of sulfate in the Northern Europe. However, it may be due to an overestimation of north boundary conditions (as the stations in Northern Europe are close to the limit of the

30 domain), a lack of deposition or errors on meteorological data that create the same overestimation than for sea salts.

Figure 5 shows the seasonal evolution of the statistics for SO$_4$ by regions.

Like Na, SO$_4$ concentrations seem to be underestimated for the stations in the Southern Europe (mostly stations in Spain) in summer and overestimated in winter and late autumn with a MFB between -30% and 40%. However, this behavior is probably not due to sulfate from sea salts (due to the low contribution of sea salt to sulfate, only a small part of sulfate would be originat-

Geoscientific
Model Development
Discussions

ing from sea salts). In Western, Central and Eastern Europe the model succeeds in reproducing the seasonal evolution with a
MFB generally between ± 30% and MFE below 50% except for Western Europe in late autumn where MFB exceeds 50% and
for Central Europe in November where MFB reaches 40%. SO_4 concentrations seem to be slightly relatively overestimated
with a MFB>0 in Eastern Europe whereas MFB is between ± 30% for Central and Western Europe. In Northern Europe, like
5 sea salts, concentrations of SO_4 are overestimated with a MFB higher than 30% and reaching 90%.

3.3 Ammonium and nitrate

Annual scores for NO_3 and NH_4 are given in Table 5. Comparisons of NO_3 and NH_4 are carried out over 37 and 33 stations
respectively. The model gives higher mean values than measurements (1.99 μg m^{-3} against 1.46 μg m^{-3} for NO_3 and 1.29
10 μg m^{-3} against 0.89 μg m^{-3} for NH_4. This kind of overestimation have been reported for numerous models (Bessagnet et al.,
2014; Lecœur and Seigneur, 2013). RMSE are higher than mean measured concentrations (1.87 μg m^{-3} and 0.97 μg m^{-3})
due to the high bias. The performance criteria are respected but not the goal criteria for both NO_3 (MFB = 15% and MFE
= 57%) and NH_4 (MFB = 36% and MFE = 55%). However, the spatiotemporal correlation is rather high (0.71 for NO_3 and
0.71 for NH_4). Figure 6 shows the annual concentrations and MFB of NO_3 and NH_4 at each station. Both, NO_3 and NH_4 are
15 overestimated at some stations in Germany, one station near Barcelona and two stations in Eastern Europe indicating there may
be too much ammonium nitrate at these stations. NH_4 is strongly overestimated in Northern Europe which may be linked to
the overestimation of sulfate and the formation of ammonium sulfate over this region whereas NO_3 is overestimated at some
stations in Southern Europe.

Figures 7 and 8 show the seasonal evolution of the statistics for NO_3 and NH_4 by regions.

20 For Southern Europe, both NO_3 and NH_4 concentrations are overestimated significantly in November-December 2013 with
MFB exceeding 40% for NO_3 and 60% for NH_4. Concentrations of NH_4 are also overestimated from January to May with
a MFB higher than 40% whereas NO_3 is overestimated to a smaller extent. NO_3 is also a bit underestimated from June to
August. These results may indicate the formation of too high ammonium nitrate concentrations at the end of the year. For NH_4,
errors on concentrations seem related to the errors on SO_4 concentrations indicating that NH_4 may be better represented with a
25 better representation of sulfates. Monthly correlations are low for NH_4 (lower than 0.4) and slightly higher for NO_3 (between
0.4 and 0.6).

For Western Europe, results on NO_3 are very similar to the results for NH_4 with an overestimation of both NO_3 and NH_4
in November and December (MFB higher than 40% for NO_3 and higher than 60% for NH_4) and a slight overestimation for
the peak in March (MFB around 30% for both NO_3 and NH_4). All together the MFB for NH_4 is higher than the MFB for
30 NO_3 which may be due to the slight overestimation of SO_4 (and therefore the overestimation of ammonium sulfate). Monthly
correlations are a bit higher for NO_3 (higher than 0.8 for most of the year) than for NH_4 (between 0.6 and 0.8 for most of the
year).

Over Central Europe, NO_3 and NH_4 concentrations are strongly overestimated at the end of the year where high concen-
trations are simulated. NH_4 is also slightly overestimated at the beginning of the year with a MFB higher than 30%. Monthly

correlations are high (between 0.6 and 0.8) for NO_3 whereas monthly correlations are lower for NH_4 in summer (below 0.5).

The results over Eastern Europe are similar to the results of Central Europe, however NO_3 concentrations are overestimated at the beginning of the year and underestimated in Summer.

For Northern Europe, NH_4 concentrations are overestimated throughout the year with a MFB around 40% in May to August and up to 120% at the end of the year. These results are very similar to the results for SO_4. NO_3 concentrations are underestimated in summer and are strongly overestimated for the rest of the year (especially in February with a MFB close to 100%).

Generally, statistics for SO_4 and NO_3 seem better than the statistics for NH_4, this may be due to the cumulative errors on ammonium nitrate and ammonium sulfate. To investigate the highlighted results on ammonium and nitrate, scores were computed for total nitrate TNO_3 (particulate NO_3 + gaseous HNO_3) and for total ammonium TNH_4 (particulate NH_4 + gaseous NH_3). The performances are close to the goal criteria with a slight overestimation of concentrations. The mean seasonal evolutions of TNO_3 and TNH_4 are plotted in Figure 9. TNO_3 and TNH_4 share the same pattern with a slight underestimation of concentrations in summer and an overestimation of concentrations in autumn and winter.

This feature could be explained by:

– An overestimation of the gas-particle conversion of HNO_3 and NH_3. Indeed, Peters and Bruckner-Schatt (1995) measured higher deposition velocity of HNO_3 and NH_3 over spruce stand and Seinfeld and Pandis (1998) reported higher deposition velocity for gases than for particles lower than 2.5 μm over water surfaces. An overestimation of the partitioning can therefore lead to an overestimation of total concentrations because the deposition velocity of these gases are generally higher than those of particles (Peters and Bruckner-Schatt, 1995).

– An underestimation of the deposition velocity.

– An overestimation of HNO_3 production rate by the gas-phase mechanism MELCHIOR 2, leading to an overestimation of the partitioning of NH_3 and HNO_3 toward the particle phase and therefore leading to an overestimation of both TNO_3 and TNH_4.

– An overestimation of NH_3 emissions in winter and autumn and an underestimation of NH_3 emissions in summer. An overestimation of NH_3 would lead to an overestimation of the partitioning of NH_3 and HNO_3 toward the particle phase and therefore lead to an overestimation of both TNO_3 and TNH_4.

The last assumption seems to be supported by the shape of the seasonal profile of NH_3 emissions used in CHIMERE illustrated in Figure 10 which gives high emissions in November-December whereas Skjøth et al. (2011) (who developed a dynamical method to estimate NH_3 emissions based on the different types of agriculture) estimated very low emissions during this period. Using dynamical emissions may give a better representation of NH_3 and NO_3 concentrations. Moreover, in some countries from Northern Europe like Sweden, NH_3 emissions are mainly due to livestock (87 % of ammonia emissions in Sweden) whereas the temporal profile for Sweden is similar to the one of other countries with two peaks of emissions (one in March-April and one in October-November) corresponding to the application of fertilizers in Spring and Autumn. It could explain why for Northern

14

Europe, NO_3 is significantly underestimated in summer and significantly overestimated at the beginning and the end of the year.

3.3.1 Organic aerosol

Organic Aerosol concentration measurements are not available in the database. However, measurements for organic carbon
5 (OC) concentrations are available. OC is the mass of carbon inside the organic aerosols. For the comparison, OM/OC ratios
(that depend on the composition of organic aerosols, especially the degree of oxidation of compounds) have to be assumed to
estimate OC concentrations from modeled OM concentrations. Turpin and Lim (2001) measured the OM/OC ratios at different
locations and found ratios between 1.2 and 2.5 and recommended to use a ratio of 2.1 for rural areas. Following Couvidat
et al. (2012), OC concentrations were calculated directly from the concentrations of each organic surrogate compounds using
10 their molecular structure to estimate the OM/OC ratio of the surrogate compounds. Several sensitivity tests were conducted by
Couvidat et al. (2012) and has shown that the OM/OC simulated by the H^2O mechanism is generally quite low compared to the
OM/OC ratio recommended by Turpin and Lim (2001). An overestimation of OC concentrations by the model could therefore
be due to an underestimation of the OM/OC ratio.

    Table 6 shows the annual statistics for organic carbon (OC) for each station. Time series of the concentrations for each
15 station are shown in Figures 12 and 13 for stations in the southern half and northern half of Europe respectively. Figure 11
shows the maps of OC concentrations over Europe for January and July 2013 as well as the MFB at stations. These figures
show for January and July an underestimation of OC concentrations over Central Europe.

    Annual concentrations at some stations seem to be overestimated (ES1778R, IT0004R and DE0003R) with MFB between
36% and 40%. However, the performance criteria is respected for these stations. It could also be possible that the overestimation
20 of OC concentrations at these stations do not correspond to an underestimation of OC if the OM/OC ratio is underestimated.
The performance goal is respected for stations CH0002R and SI0008R whereas the performance criteria are respected for
stations CY0002R, DE0008R, PL0005R and SE0011R. Concentrations are underestimated at the other stations with MFB
between -56% and -87%.

    Although OC concentrations are slightly overestimated in ES1778 (near Barcelona, Spain) and IT0004 (in Ispra, Italy) the
25 seasonality of OC concentrations is well captured by the model. Moreover, the overestimation of concentrations could be due to
the proximity of high emissions sources and the low resolution of the model (ES1778 is only at 50 km from Barcelona whereas
the resolution is only of 0.25° and IT0004 is close to Milan). Concentrations and the seasonal evolution are well reproduced in
SI0008 (Iskbra, Slovenia). For the other stations in the south of Europe, summer concentrations are underestimated in summer
whereas the winter concentrations seem to be well reproduced. This may indicate a lack of secondary organic aerosol formation.
30 These stations all have strong modeled concentrations of biogenic SOA in summer and strong modeled concentrations of
anthropogenic organic aerosol in winter.

    For the northern half of Europe, except for stations DE0003 (for which concentrations are overestimated in Winter), the
station CH0005R in Switzerland and PL0005R in Poland, summer concentrations of organic aerosol are underestimated. Only

a peak of organic aerosol (due to biogenic aerosols in the model) at the end of August for several stations (CZ0003R, DE0002R, DE0007R, DE0008R, DE0044R) is well reproduced by the model.

3.3.2 PM concentrations

Annual scores for $PM_{2.5}$ and PM_{10} are given in Table 5. Comparisons are carried out over 41 stations for $PM_{2.5}$ and 59 stations
for PM_{10}. The goal criteria is respected for both $PM_{2.5}$ and PM_{10}. However, $PM_{2.5}$ concentrations are slightly overestimated (MFB = 22%). The MFB for PM_{10} is lower (8%) indicating that coarse particles may be underestimated. This is confirmed by the fact that for the stations with measurements of both $PM_{2.5}$ and PM_{10}, the MFB for $PM_{2.5}$ (17%) is higher than the MFB for PM_{10} (4%). The underestimation of coarse particles was reported for numerous models in the intercomparison model projet AQMEII (Solazzo et al., 2012; Pirovano et al., 2012).

The simulated mean concentrations (10.54 μg m^{-3} for $PM_{2.5}$ and 14.42 μg m^{-3} for PM_{10}) are close to the measured mean concentrations (9.06 μg m^{-3} for $PM_{2.5}$ and 13.51 μg m^{-3} for PM_{10}) and the spatiotemporal correlations are high (0.68 for $PM_{2.5}$ and 0.60 for PM_{10}).

Figure 14 shows the annual concentrations and MFB of $PM_{2.5}$ and PM_{10} at each station. The model strongly underestimates annual concentrations of PM_{10} only for the ES0008R station, probably due to the underestimation of sea salt at this station. However, the model overestimates PM concentrations with a MFB above 30% at several locations (14 stations for $PM_{2.5}$ and 12 stations for PM_{10} especially over the Alps).

Figures 15 and 17 show the seasonal evolution of the statistics by regions for $PM_{2.5}$ and PM_{10}, respectively.

$PM_{2.5}$ concentrations seem to be underestimated for the stations in the Southern Europe from June to August and overestimated the rest of the year (especially in March, November and December with MFB reaching 60%). A similar feature is obtained with PM_{10} but with lower MFB in March, November and December, which is probably due to some compensation effects and an underestimation of the coarse fraction of PM. Based on these results, this overestimation is probably mainly due to the overestimation of ammonium nitrate observed during these months while the underestimation from June to August is probably due to the underestimation of all PM components.

For Western Europe, $PM_{2.5}$ are overestimated from September to December with a MFB between 40% and 60% which may be due at least partly to the overestimation of ammonium nitrate. The overestimation could also be due to an overestimation of organic matter observed at some stations or to an overestimation of primary particles. Similar results are obtained for PM_{10}.

In Central Europe, the model reproduces well the strong concentrations of $PM_{2.5}$ and PM_{10} in Winter and Spring (with a MFE around 40%). However, concentrations are slightly underestimated in summer (with a negative MFB reaching -30% for $PM_{2.5}$ and -40% for PM_{10}) and are overestimated from October to December with a MFB between 40% and 80% for $PM_{2.5}$ (probably due to the strong overestimation of ammonium nitrate) and reaching 50% for PM_{10}.

For Eastern and Northern Europe, similar features are obtained. $PM_{2.5}$ and PM_{10} are overestimated in Winter and Fall (probably due to mostly to the overestimation of ammonium nitrate) and underestimated in Summer (probably due to the summer underestimation of ammonium nitrate and organic aerosols).

A Quantile-Quantile (QQ) scatter plot of modeling results against measurements for PM_{10} and $PM_{2.5}$ is shown in Figure

Geoscientific
Model Development
Discussions

16. QQ plots can be used to assess the similarity of the distribution of two compared datasets. For Southern Europe, concentrations higher than 40 μg m^{-3} for PM$_{10}$ and higher than 20 μg m^{-3} for PM$_{2.5}$ are significantly underestimated, especially for high concentrations of PM$_{2.5}$. Western Europe and Central Europe have a similar distribution of concentrations with a strong overestimation of high concentrations of PM$_{2.5}$ (higher than 35 μg m^{-3}) and of PM$_{10}$ (higher than 55 μg m^{-3}). This overestimation is probably due to the high overestimation of ammonium nitrate during the late autumn for these regions. For Eastern Europe and Southern Europe, the distributions of modeled concentrations are similar to the distributions of observed concentrations.

3.3.3 Case of the Cyprus station

The Cyprus station (CY0002R) was analyzed due to the specificities of this station close to the boundary conditions, influenced by high concentrations of PM due to mineral dusts and high anthropogenic emissions from the Mediterranean maritime traffic. Morever, numerous measurements were carried out at this station: PM$_{2.5}$ and PM$_{10}$ and measurements of speciation (both in the fine fraction and in PM$_{10}$) covering NO$_3$, NH$_4$, SO$_4$, Na, Cl and also Ca (originating mainly from dust). The temporal evolution of PM$_{2.5}$ and PM$_{10}$, Ca (fine fraction and total), NO$_3$ (fine fraction and total) are shown in Figure 18 and the temporal evolution of Na, Cl, NH$_4$ and SO$_4$ are shown in Figure 19. The temporal evolution of OC concentrations is shown in Figure 13.

The model gives at this station good performances for the simulation of PM$_{2.5}$ (correlation = 0.54, MFB=-10%, MFE=35%) and PM$_{10}$ (correlation=0.64, MFB=26%, MFE=39%). The temporal evolution of PM$_{2.5}$ and PM$_{10}$ are well reproduced by the model. The good results at this station are mainly due to the good representation of dusts transport in the simulation (coming here from the boundary conditions taken from Mozart v4.0). Simulated concentrations of Ca (assuming a fraction of 6% in dusts) were compared to the measurements of Ca. The model gives good results for Ca concentrations in PM10 (correlation=0.65, MFB=6% and MFE=45%) but Ca concentrations in fine particles are overestimated (correlation=0.53, MFB=63% and MFE=81%) but the concentrations (0.19 μg m^{-3} in measurements) are low compared to Ca in PM10 (1.32 μg m^{-3} in measurements). Na and Cl are strongly underestimated (MFB=-85% and MFB=-40% for Cl).

The model almost respects the goal criteria for NO$_3$ in PM$_{10}$ (MFB=24% and MFE=51%) but with a low correlation (0.38). The modeled annual mean of NO$_3$ in PM$_{10}$ (1.66 μg m^{-3}) is close to the measured annual mean (1.53 μg m^{-3}). However, the measured annual mean of NO$_3$ in fine particles is strongly overestimated (0.71 μg m^{-3} against 0.18 μg m^{-3}). The model seems here to underestimate the coarse faction of NO$_3$. Even if the model gives strong NO$_3$ concentrations in the coarse fraction due to the coarse mode formation with dusts, a significant part of NO$_3$ in the model seems to be due to ammonium nitrate formation in PM whereas most of NH$_4$ seems to be due to ammonium sulfate formation (correlation of 0.85 between observed sulfate and ammonium). A similar feature is observed at station ES0008R with a good order of magnitude for NO$_3$ in PM$_{10}$ (1.23 μg m^{-3} in the model and 1.19 μg m^{-3} in measurements) but with an overestimation of NO$_3$ in the fine fraction (1.22 μg m^{-3} in the model and 0.38 μg m^{-3} in measurements). These results may be partly due to a lack of HNO$_3$ condensing onto dusts but the underestimation is probably mainly due to sea salts which are underestimated at these two stations.

NH$_4$ concentrations are overestimated (probably due to the overestimation of ammonium nitrate and the lack of HNO$_3$ con-

densing onto dusts) with a MFB of 49% whereas SO_4 concentrations are underestimated (MFB=-0.29%) especially in July and November 2013 where the model is not able to reproduce the high concentrations of sulfate. Correlation are very low (0.23 for NH_4 and 0.13 for SO_4).

5 3.3.4 Case of the Melpitz station (Germany)

Numerous simultaneous types of measurements were also carried out at the Melpitz station (DE0044R) in Germany. The temporal evolution of $PM_{2.5}$ and PM_{10}, Ca (fine fraction and total), NO_3 (fine fraction and total) are shown in Figure 20 and the temporal evolution of Na, Cl, NH_4, SO_4 and elemental carbon (EC) are shown in Figure 21. The temporal evolution of OC concentrations is shown in Figure 12

10   At this station, $PM_{2.5}$ and PM_{10} share a similar pattern. For $PM_{2.5}$, annual concentrations are underestimated by the model (13.2 μg m^{-3} against 17.8 μg m^{-3} in measurements) especially in summer with an underestimation ranging from 7 and 11 μg m^{-3} from June to August and a monthly MFB between -65% and -95% and in a lesser extent in winter (except in February) with an underestimation of about 7 μg m^{-3}. For PM_{10}, the underestimation is stronger (15.7 μg m^{-3} against 22.1 μg m^{-3}) especially between april and august with an underestimation between 10 and 15 μg m^{-3}.

15   Concentrations of SO_4 are well reproduced by the model with a high correlation (0.83) and low MFB and MFE (0.12% and 0.35%). The model succeeds to capture the high concentrations of SO_4 in winter. NO_3 concentrations and NH_4 concentrations are also well reproduced by the model except at the end of the year where concentrations are strongly overestimated. The high concentrations of NO_3 in February and March are well reproduced by the model (temporal correlation of 0.91 and 0.73, MFE=30% and 40%). The low concentrations of Na and Cl are a bit overestimated. The overestimation reaches 0.34 μg m^{-3}
20   for Na and 0.41 μg m^{-3} for Cl in January.

Most of the underestimation of $PM_{2.5}$ concentrations is probably due to the underestimation of organic aerosols at this station. Indeed, OC concentrations are underestimated by 2.9 μg m^{-3} from June to August. Using the OM/OC ratio of 2.1 measured by Turpin and Lim (2001) for rural areas, the underestimation of organic aerosol could explain most of the differences between modeled and measured $PM_{2.5}$. However, in June, the underestimation of OC concentrations is only of 3.3 μg
25   m^{-3} which would correspond to an underestimation of OM of 7 μg m^{-3} whereas $PM_{2.5}$ concentrations are underestimated by 11 μg m^{-3}. It appears difficult that in June, the underestimation alone of organic aerosols could explain all the underestimation of PM. The remaining underestimation in June cannot be explained by SO_4, NO_3, NH_4, Na or Cl. The sum of these concentrations is 4.0 μg m^{-3} for the model and 3.0 μg m^{-3} for measurements. The fine fraction of Ca is a bit underestimated by the model (0.08 μg m^{-3} against 0.11 μg m^{-3} in measurements), which could explain an underestimation of 0.75 μg m^{-3}
30   (assuming that there is 4% of Ca in dusts) which is just enough to compensate the overestimation by the model of inorganic aerosols. The remaining underestimation in June could be explain by an underestimation of primary aerosols. However, EC concentrations are well reproduced by the model (annual correlation of 0.62, MFB=0.34% and MFE=47%) and are slightly overestimated by the model (0.42 μg m^{-3} against 0.22 μg m^{-3} in measurements).

4   Perspectives on model improvement

The following list provides a list of possible developments that may be addressed in the future:

– The formation of ammonium nitrate in the model for which the strongest errors were obtained need to be improved. As NH_3 emissions is a key element, implementing a dynamic method to improve the spatial and temporal evolution of NH_3 emissions from agriculture like the method described in Skjøth et al. (2011) depending on temperature and wind speed could be a major improvement.

– The formation of anthropogenic SOA has to be better represented in the model. For that, SVOC and IVOC emissions should be better represented. The inventory of Denier van der Gon et al. (2015) could be used to better estimate SVOC from residential biomass burning. More generally, to take into IVOC emissions, emission inventory by volatility classes should be developed based for example on the method developed by Zhao et al. (2016b). Moreover, mechanisms of formation of SOA from IVOC oxidation and the aging of SVOC have to be better understood. Bruns et al. (2016) showed that the formation of SOA from SOA precursors traditionally taken into account in models (like toluene, xylene, alkanes) only amount for a small amount of SOA (between 3 and 27% of SOA formed) from biomass burning and that most of the SOA is due to non-traditional SOA precursors (like phenol, naphthalene, benzaldehyde, etc...). These precursors should be added in the SOA mechanism. Aging has also a major impact on SOA formation (Donahue et al., 2012; Zhao et al., 2016a) and should be studied into greater details.

– The influence of the gas-phase mechanism on PM formation should be tested within CHIMERE. Indeed, Sarwar et al. (2013) found significant differences over the United States of America between CB05 (Sarwar et al., 2008) and RACM2 (Goliff et al., 2013) in OH concentrations (46% in OH concentrations) and PM components (10 % in sulfate, 6% in nitrate, 10% in ammonium, 42% in anthropogenic SOA and 5% in biogenic SOA). The strong differences in radical concentrations may strongly affect the aging of SVOC compounds and the seasonal evolution of PM components. It may also be important to compare the results of the MELCHIOR 2 mechanisms with more recent gas-phase mechanisms.

– The formation of inorganic aerosol could be integrated in the SOAP thermodynamic model. SOAP would then be able to simulate both inorganic and organic aerosols and take into account the influence between inorganic and organic aerosols which can affect the partitioning of compounds and the hygroscopicity of the aerosol (Jing et al., 2016). This could also be important to take into account the formation of some acid organics/ammonium salts which can be in competition with ammonium nitrate formation. Some organonitrogen compounds were also found by condensation of ammonia onto organic aerosols (Liu et al., 2015).

– Some recent experimental studies emphasize the need to account for dynamical aspects of the organic aerosols formation rather than assuming thermodynamic equilibrium with the gas phase because organic aerosols can be highly viscous (Virtanen et al., 2010; Cappa and Wilson, 2011; Pfrang et al., 2011; Shiraiwa et al., 2011; Vaden et al., 2011; Shiraiwa and Seinfeld, 2012; Abramson et al., 2013). To our knowledge, this phenomenon was never investigated inside a 3D air

quality model. However, to take it into account, a dynamic method for SOA formation taking into account the diffusion inside a few layers was developed in the thermodynamic model SOAP. This method could be used to test the influence of the organic-phase viscosity on SOA formation inside a 3D air quality model.

- Aqueous-phase chemical mechanism can be extensively improved. Several studies highlight the importance of aqueous-phase chemistry for SOA formation from isoprene. An isoprene-derived epoxidiol (IEPOX) has been shown to form methyltetrols and C_5-alkene triols in the aqueous phase of particles and droplets by hydrolysis as well as organosulfates by reaction with sulfate or bisulfate ions and oligomers (Surratt et al., 2010). Froyd et al. (2010) found very high concentrations of SOA formed from IEPOX in Atlanta, USA (910 ng.m^{-3}), due to a very acidic aerosol. The formation of SOA from IEPOX was investigated in a previous study (Couvidat et al., 2013). Using a Henry's law constant of IEPOX of 2×10^7 M/atm and a mechanism based on available information, the model could simulate concentrations of SOA from IEPOX in the right order of magnitude and simulates concentrations of SOA from IEPOX in summer that could could reach 1 μg m^{-3} over some regions and could give strong peaks of SOA. Nguyen et al. (2014) found a Henry's law constant of 3×10^7 M/atm. However, this modeling study did not take into account interactions with inorganics aerosol. Aqueous-phase processing of glyoxal (which is formed from the oxidation of toluene and isoprene) was also found to be possibly a significant source of SOA as it can form oxalic acid via reaction in clouds (Griffin et al., 2003) and could form oligomers or form SOA in particles via reaction with hydroxyl radical or from reactions catalysed by ammonium (Knote et al., 2014) which could be important to take into account. Implementing a complete cloud chemical mechanism should be tested. A mechanism similar to Leriche et al. (2013) could be implemented to improve the representation of the cloud chemistry inside the model.

- The number of particles has also an effect on health, especially in urban areas (Jing et al., 2001). To properly estimate the effects on health of particles in urban areas, more complete parameterization of nucleation should be implemented (taking for example the impact of organic compounds (Lupascu et al., 2015)) and model results should be compared to available data on European Megacities.

- The possibility to take into account the mixing state (as done by Zhu et al. (2015, 2016); S. et al. (2016) should be added to the model as it can impact the aerosol formation and composition and their optical and hygroscopic properties.

5 Conclusions

Concentrations were compared to available information on PM concentrations and composition thanks to the EBAS database. Whereas the model gives satisfactory results in regard of the criteria defined by Boylan and Russell (2006), results could be improved in terms of seasonality and PM composition. Strongest errors were found to be probably due to ammonium nitrate which is often overestimated especially in late autumn (probably due to an overestimation of NH_3 emissions during this period). Only in summer, concentrations of ammonium nitrate could be underestimated. Strong errors were also found on OC concentrations in summer (especially over the northern half of Europe) indicating that strong concentrations of anthropogenic

SOA could be missing from the models. Sea salts concentrations were properly simulated at most stations but were overestimated over regions with low concentrations and underestimated for regions with very strong concentrations (which could lead to an underestimation of HNO_3 condensation onto coarse particles).

However, the model has good performances in general and respects the goal criteria for both $PM_{2.5}$ and PM_{10}. For sea salts, the model almost respects the goal criteria of Boylan and Russell (2006) and succeed in reproducing the seasonal evolution of concentrations for Western and Central Europe. For sulfate, except for an overestimation of sulfate in Northern Europe, modeled concentrations are close to observations with a good seasonal evolution of concentrations. For organic aerosol, the model performs well for stations with strong modeled biogenic SOA concentrations.

Several improvements should be tested. Taking into account the dynamic of NH_3 emissions could greatly improve the results of the model in simulating ammonium nitrate. Taking into account SOA formation from missing SVOC/IVOC emissions probably has an important impact on SOA formation and could probably improve results on SOA concentrations. Moreover, the impact of inorganic-organic interactions and the effect of aqueous-phase chemistry on SOA formation should be investigated.

6   Code availability

Chimere2017β is a version of chimere developed for research on aerosol modeling. It is available on request by contacting the authors.

Geoscientific
Model Development
Discussions

References

Abramson, E., Imre, D., Beránek, J., Wilson, J., and Zelenyuk, A.: Experimental determination of chemical diffusion with secondary organic aerosol particles, Phys. Chem. Chem. Phys., 15, 2983–2991, doi:10.1039/C2CP44013J, 2013.

Ansari, A. S. and Pandis, S. N.: Prediction of multicomponent inorganic atmospheric aerosol behavior, Atmos. Environ., 33, 745–757, doi:10.1016/S1352-2310(98)00221-0, 1999.

Bessagnet, B., Menut, L., Curci, G., Hodzic, A., Guillaume, B., Liousse, C., Moukhtar, S., Pun, B., Seigneur, C., and Schulz, M.: Regional modeling of carbonaceous aerosols over Europe-focus on secondary organic aerosols, J. Atmos. Chem., 61, 175–202, doi:10.1007/s10874-009-9129-2, 2008.

Bessagnet, B., Seigneur, C., and Menut, L.: Impact of dry deposition of semi-volatile organic compounds on secondary organic aerosols, Atmos. Environ., 44, 1781–1787, doi:10.1016/j.amtosenv.2010.01.027, 2010.

Bessagnet, B., Colette, A., Meleux, F., Rouïl, L., Ung, A., Favez, O., Thunis, P., Cuvelier, C., Tsyro, S., Stern, R., Manders, A., Kranenburg, R., Aulinger, A., Bieser, J., Mircea, M., Briganti, G., Cappelletti, A., Calori, G., Finardi, S., Silibello, C., Ciarelli, G., Aksoyoglu, S., Prévot, A., Pay, M.-T., Baldasano, J., García Vivanco, M., Garrido, J. L., Palomino, I., Martín, F., Pirovano, G., Roberts, P., Gonzalez, L., White, L., Menut, L., Dupont, J.-C., Carnevale, C., and Pederzoli, A.: The EURODELTA III exercise – Model evaluation with observations issued from the 2009 EMEP intensive period and standard measurements in Feb/Mar 2009, Tech. rep., EMEP, 2014.

Bessagnet, B., Pirovano, G., Mircea, M., Cuvelier, C., Aulinger, A., Calori, G., Ciarelli, G., Manders, A., Stern, R., Tsyro, S., García Vivanco, M., Thunis, P., Pay, M.-T., Colette, A., Couvidat, F., Meleux, F., Rouïl, L., Ung, A., Aksoyoglu, S., Baldasano, J. M., Bieser, J., Briganti, G., Cappelletti, A., D'Isidoro, M., Finardi, S., Kranenburg, R., Silibello, C., Carnevale, C., Aas, W., Dupont, J.-C., Fagerli, H., Gonzalez, L., Menut, L., Prévôt, A. S. H., Roberts, P., and White, L.: Presentation of the EURODELTA III intercomparison exercise – evaluation of the chemistry transport models' performance on criteria pollutants and joint analysis with meteorology, Atmos. Chem. Phys., 16, 12 667–12 701, doi:10.5194/acp-16-12667-2016, 2016.

Boylan, J. W. and Russell, A. G.: PM and light extinction model performance metrics, goals, and criteria for three-dimensional air quality models, Atmos. Environ., 40, 4946–4959, doi:10.1016/j.atmosenv.2005.09.087, 2006.

Bruns, E. A., El Haddad, I., Slowik, J. G., Kilic, D., Klein, F., Baltensperger, U., and Prévôt, A. S. H.: Identification of significant precursor gases of secondary organic aerosols from residential wood combustion, Scientific Reports, 6, 27 881, doi:10.1038/srep27881, 2016.

Cappa, C. D. and Wilson, K. R.: Evolution of organic aerosol mass spectra upon heating: implications for OA phase and partitioning behavior, Atmos. Chem. Phys., 11, 1895–1911, doi:10.5194/acp-11-1895-2011, 2011.

Carlton, A. G., Bhave, P. V., Napelenok, S. L., Edney, E. O., Sarwar, G., Pinder, R. W., Pouliot, G. A., and Houyoux, M.: Model Representation of Secondary Organic Aerosol in CMAQv4.7, Environ. Sci. Tech., 44, 8553–8560, doi:10.1021/es100636q, 2010.

Chan, A. W. H., Kautzman, K. E., Chhabra, P. S., Surratt, J. D., Chan, M. N., Crounse, J. D., Kürten, A., Wennberg, P. O., Flagan, R. C., and Seinfeld, J. H.: Secondary organic aerosol formation from photooxidation of naphthalene and alkylnaphthalenes: implications for oxidation of intermediate volatility organic compounds (IVOCs), Atmos. Chem. Phys., 9, 3049–3060, doi:10.5194/acp-9-3049-2009, 2009.

Couvidat, F. and Sartelet, K.: The Secondary Organic Aerosol Processor (SOAP v1.0) model: a unified model with different ranges of complexity based on the molecular surrogate approach, Geosci. Model Dev., 8, 1111–1138, doi:10.5194/gmd-8-1111-2015, 2015.

Couvidat, F. and Seigneur, C.: Modeling secondary organic aerosol formation from isoprene oxidation under dry and humid conditions, Atmos. Chem. Phys., 11, 893–909, doi:10.5194/acp-11-893-2011, 2011.

Geoscientific
Model Development
Discussions

Couvidat, F., Debry, É., Sartelet, K., and Seigneur, C.: A Hydrophilic/Hydrophobic Organic (H²O) model: Model development, evaluation and sensitivity analysis, J. Geophys. Res., 117, D10 304, doi:10.1029/2011JD017214, 2012.

Couvidat, F., Sartelet, K., and Seigneur, C.: Investigating the impact of aqueous-phase chemistry and wet deposition on organic aerosol formation using a molecular surrogate modeling approach, Environ. Sci. Technol., 47, 914–922, doi:10.1021/es3034318, 2013.

5 Croft, B., Lohmann, U., Martin, R. V., Stier, P., Wurzler, S., Feichter, J., Hoose, C., Heikkilä, U., van Donkelaar, A., and Ferrachat, S.: Influences of in-cloud aerosol scavenging parameterizations on aerosol concentrations and wet deposition in ECHAM5-HAM, Atmos. Chem. Phys., 10, 1511–1543, doi:10.5194/acp-10-1511-2010, 2010.

de Wolf, A. D.: On the Laws-Parsons distribution of raindrop sizes, Radio Sci., 36, 639–642, doi:10.1029/2000RS002369, 1999.

Debry, E., Fahey, K., Sartelet, K., Sportisse, B., and Tombette, M.: Technical Note: A new SIze REsolved Aerosol Model (SIREAM), Atmos.

10 Chem. Phys., 7, 1537–1547, doi:10.5194/acp-7-1537-2007, 2007.

Denier van der Gon, D., Bergström, R., Fountoukis, C., Johansson, C., Pandis, S. N., Simpson, D., and Visschedijk, A. J. H.: Particulate emissions from residential wood combustion in Europe – revised estimates and an evaluation, Atmos. Chem. Phys., 15, 6503–6519, doi:10.5194/acp-15-6503-2015, 2015.

Donahue, N. M., Henry, K. M., Mentel, T. F., Kiendler-Scharr, A., Spindler, C., Bohn, B., Brauers, T., Dorn, H. P., Fuchs, H., Tillmann, R.,

15 Wahner, A., Saathoff, H., K.-H., N., Möhler, O., Leisner, T., Müller, L., Reinnig, M.-C., Hoffmann, T., Salo, L., Hallquist, M., Frosch, M., Bilde, M., Tritscher, T., Barmet, P., Praplan, A. P., DeCarlo, P. F., Dommen, J., Prévôt, A. S. H., and Baltensperger, U.: Aging of biogenic secondary organic aerosol via gas-phase OH radical reactions, Proc. Natl. Acad. Sci., 109, 13 503–13 508, doi:10.1073/pnas.1115186109, 2012.

Emmons, L. K., Walters, S., Hess, P. G., Lamarque, J. F., Pfister, G. G., Fillmore, D., Granier, C., Guenther, A., Kinnison, D., Laepple, T.,

20 Orlando, J., Tie, X., Tyndall, G., Wiedinmyer, C., Baughcum, S. L., and Kloster, S.: Description and evaluation of the Model for Ozone and Related chemical Tracers, version 4 (MOZART-4), Geosci. Model Dev., 3, 43–67, doi:10.5194/gmd-3-43-2010, 2010, 2010.

Formenti, P., Rajot, J. L., Desboeufs, K., Caquineau, S., Chevaillier, S., Nava, S., Gaudichet, A., Journet, E., Triquet, S., Alfaro, S., Chiri, M., Haywood, J., Coe, H., and Highwood, E.: Regional variability of the composition of mineral dust from western Africa: Results from the AMMA SOP0/DABEX and DODO field campaigns, J. Geophys. Res., 113, D00C13, doi:10.1029/2008JD009903, 2008.

25 Fountoukis, C. and Nenes, A.: ISORROPIA II: a computationally efficient thermodynamic equilibrium model for K^+–Ca^{2+}–Mg^{2+} –NH_4^+–Na^+–SO_4^{2-}–NO_3^-–Cl^-–H_2O aerosols, Atmos. Chem. Phys., 7, 4639–4659, doi:10.5194/acp-7-4639-2007, 2007.

Fredenslund, A., Jones, R. L., and Prausnitz, J. M.: Group-contribution estimation of activity-coefficients in nonideal liquid-mixtures, AIChE J., 21, 1086–1099, 1975.

Froyd, K. D., Murphy, S. M., Murphy, D. M., de Gouw, J. A., Eddingsaas, N. C., and Wennberg, P. O.: Contribution of isoprene-derived

30 organosulfates to free tropospheric aerosol mass, Proc. Natl. Acad. Sci., 107, 21 360–21 365, doi:10.1073/pnas.1012561107, 2010.

Ganbavale, G., Zuend, A., Marcolli, C., and Peter, T.: Improved AIOMFAC model parameterisation of the temperature dependence of activity coefficients for aqueous organic mixtures, Atmos. Chem. Phys., 15, 447–493, doi:10.5194/acp-15-447-2015, 2015.

Goliff, W. S., Stockwell, W. R., and Lawson, C. V.: The Regional Atmospheric Chemistry Mechanism, Version 2, Atmos. Environ., 68, 174–185, 2013.

35 Grieshop, A. P., Logue, J. M., Donahue, N. M., and Robinson, A. L.: Laboratory investigation of photochemical oxidation if organic aerosol from wood fires. 1: measurement and simulation of organic aerosol evolution, Atmos. Chem. Phys., 9, 1263–1277, doi:10.5194/acp-9-1263-2009, 2009.

Griffin, R. J., Nguyen, K., Dabdub, D., and Seinfeld, J. H.: A coupled hydrophobic-hydrophilic model for predicting secondary organic aerosol formation, J. Atmos. Chem., 44, 171–190, doi:10.1023/A:1022436813699, 2003.

Guenther, A. B., Jiang, X., Heald, C. L., Sakulyanontvittaya, T., Duhl, T., Emmons, L. K., and Wang, X.: The Model of Emissions of Gases and Aerosols from Nature version 2.1 (MEGAN2.1): an extended and updated framework for modeling biogenic emissions, Geosci. Model

5   Dev., 5, 1471–1492, doi:10.5194/gmd-5-1471-2012, 2012.

Henzing, J. S., Olivié, D. J. L., and van Velthoven, P. F. J.: A parameterization of size resolved below cloud scavenging of aerosols by rain, Atmos. Chem. Phys., 6, 3363–3375, doi:10.5194/acp-6-3363-2006, 2006.

Hodzic, A., Bessagnet, B., and Vautard, R.: A model evaluation of coarse-mode nitrate heterogeneous formation on dust particles, Atmos. Environ., 40, 4158–4171, doi:10.1016/j.atmosenv.2006.02.015, 2006.

10   Jacobson, M. Z. and Turco, R. P.: Modeling coagulation among particles of different composition and size, Atmos. Environ., 28, 1327–1338, doi:10.1016/1352-2310(94)90280-1, 1994.

Jing, B., Tong, S., Liu, Q., Li, K., Wang, W., Zhang, Y., and Ge, M.: Number concentration and size of particles in urban air: effects on spirometric lung function in adult asthmatic subjects, Environ. Health Perspect., 109, 319–323, 2001.

Jing, B., Tong, S., Liu, Q., Li, K., Wang, W., Zhang, Y., and Ge, M.: Hygroscopic behavior of multicomponent organic aerosols and their

15   internal mixtures with ammonium sulfate, Atmos. Chem. Phys., 16, 4101–4118, doi:10.5194/acp-16-4101-2016, 2016.

Kanakidou, M., Seinfeld, J. H., Pandis, S. N., Barnes, I., Dentener, F. J., Facchini, M. C., Van Dingenen, R., Ervens, B., Nenes, A., Nielsen, C. J., Swietlicki, E., Putaud, J. P., Balkanski, Y., Fuzzi, S., Horth, J., Moortgat, G. K., Winterhalter, R., Myhre, C. E. L., Tsigaridis, K., Vignati, E., Stephanou, E. G., and Wilson, J.: Organic aerosol and global climate modelling: a review, Atmos. Chem. Phys., 5, 1053–1123, doi:10.5194/acp-5-1053-2005, 2005.

20   Kautzman, K. E., Surratt, J. D., Chan, M. N., Chan, A. W. H., Hersey, S. P., Chhabra, P. S., Dalleska, N. F., Wennberg, P. O., Flagan, R. C., and Seinfeld, J. H.: Chemical composition of gas- and aerosol-phase products from the photooxidation of naphthalene, J. Phys. Chem. A, 114, 913–934, doi:10.1021/jp908530s, 2010.

Knote, C., Hodzic, A., Jimenez, J. L., Volkamer, R., Orlando, J. J., Baidar, S., Brioude, J., Fast, J., Gentner, D. R., Goldstein, A. H., Hayes, P. L., Knighton, W. B., Oetjen, H., Setyan, A., Stark, H., Thalman, R., Tyndall, G., Washenfelder, R., Waxman, E., and Zhang, Q.: Organic

25   aerosol formation from the reactive uptake of isoprene epoxydiols (IEPOX) onto non-acidified inorganic seeds, Atmos. Chem. Phys., 14, 6213–6239, doi:10.5194/acp-14-6213-2014, 2014.

Lecœur, E. and Seigneur, C.: Dynamic evaluation of a multi-year model simulation of particulate matter concentrations over Europe, Atmos. Chem. Phys., 13, 4319–4337, doi:10.5194/acp-13-4319-2013, 2013.

Leriche, M., Pinty, J.-P., and Mari, C.: A cloud chemistry module for the 3-D cloud-resolving mesoscale model Meso-NH with application

30   to idealized cases, Geosci. Model Dev., 6, 1275–1298, doi:10.5194/gmd-6-1275-2013, 2013.

Liu, Y., Liggio, J., Staebler, R., and Li, S.-M.: Reactive uptake of ammonia to secondary organic aerosols: kinetics of organonitrogen formation, Atmos. Chem. Phys., 15, 13 569–13 584, doi:10.5194/acp-15-13569-2015, 2015.

Lupascu, A., Easter, R., Zaveri, R., Shrivastava, M., Pekour, M., Tomlinson, J., Yang, Q., Matsui, H., Hodzic, A., Zhang, Q., and Fast, J. D.: Modeling particle nucleation and growth over northern California during the 2010 CARES campaign, Atmos. Chem. Phys., 15,

35   12 283–12 313, doi:10.5194/acp-15-12283-2015, 2015.

Mätlzer, C.: Drop-size distributions and Mie computations for rain, Tech. rep., IAP research report, 2002.

Menut, L., Bessagnet, B., Khvorostyanov, D., Beekmann, M., Blond, N., Colette, A., Coll, I., Curci, G., Foret, G., Hodzic, A., Mailler, S., Meleux, F., Monge, J.-L., Pison, I., Siour, G., Turquety, S., Valari, M., Vautard, R., and Vivanco, M. G.: CHIMERE 2013: a model for regional atmospheric composition modelling, Geosci. Model Dev., 6, 981–1028, doi:10.5194/gmd-6-981-2013, 2013.

Moya, M., Pandis, S. N., and Jacobson, M. Z.: Is the size distribution of urban aerosols determined by thermodynamic equilibrium? An application to Southern California, Atmos. Environ., 36, 2349–2365, doi:10.1016/S1352-2310(01)00549-0, 2002.

Neumann, D., Matthias, V., Bieser, J., Aulinger, A., and Quante, M.: A comparison of sea salt emission parameterizations in northwestern Europe using a chemistry transport model setup, Atmos. Chem. and Phys., 16, 9905–9933, doi:10.5194/acp-16-9905-2016, 2016.

Nguyen, T. B., Coggon, M. M., Bates, K. H., Zhang, X., Schwantes, R. H., Schilling, K. A., Loza, C. L., Flagan, R. C., Wennberg, P. O., and Seinfeld, J. H.: Organic aerosol formation from the reactive uptake of isoprene epoxydiols (IEPOX) onto non-acidified inorganic seeds, Atmos. Chem. Phys., 14, 3497–3510, doi:10.5194/acp-14-3497-2014, 2014.

Nordin, E. Z., Eriksson, A. C., Roldin, P., Nilsson, P. T., Carlsson, J. E., Kajos, M. K., Hellén, H., Wittbom, C., Rissler, J., Löndahl, J., Swietlicki, E., Svenningsson, B., Bohgard, M., Kulmala, M., Hallquist, M., and Pagels, J. H.: Secondary organic aerosol formation from idling gasoline passenger vehicle emissions investigated in a smog chamber, Atmos. Chem. Phys., 13, 6101–6116, doi:10.5194/acp-13-6101-2013, 2013.

Pandis, S., Wexler, A., and Seinfeld, J.: Secondary organic aerosol formation and transport -II. Predicting the ambient secondary organic aerosol size distribution, Atmos. Environ., 27A, 2403–2416, doi:10.1016/0960-1686(93)90408-Q, 1993.

Pankow, J. F.: An absorption model of gas/particle partitioning of organic compounds in the atmosphere, Atmos. Environ., 28A, 185–188, 1994.

Peters, K. and Bruckner-Schatt, G.: The dry deposition of gaseous and participate nitrogen compounds to a spruce stand, Water, Air, and Soil Pollution, 85, 2217–2222, doi:10.1007/BF01186163, 1995.

Pfrang, C., Shiraiwa, M., and Pöschl, U.: Chemical ageing and transformation of diffusivity in semi-solid multi-component organic aerosol particles, Atmos. Chem. Phys., 11, 7343–7354, doi:10.5194/acp-11-7343-2011, 2011.

Pirovano, G., Balzarini, A., Bessagnet, B., Emery, C., Kallos, G., Meleux, F., Mitsakou, C., Nopmongcol, U., M., R. G., and Yarwood, G.: Investigating impacts of chemistry and transport model formulation on model performance at European scale, Atmos. Environ., 53, 1–17, doi::10.1016/j.atmosenv.2011.12.052, 2012.

Platt, S. M., El Haddad, I., Zardini, A. A., Clairotte, M., Astorga, C., Wolf, R., Slowik, J. G., Temime-Roussel, B., Marchand, N., Jezek, I., Drinovec, L., Mocnik, G., Möhler, O., Richter, R., Barmet, P., Bianchi, F., Baltensperger, U., and Prévôt, A. S. H.: Secondary organic aerosol formation from gasoline vehicle emissions in a new mobile environmental reaction chamber, Atmos. Chem. Phys., 13, 9141–9158, doi:10.5194/acp-13-9141-2013, 2013.

Pozzoli, L., Janssens-Maenhout, G., Diehl, T., Bey, I., Schultz, M. G., Feichter, J., Vignati, E., and Dentener, F.: Re-analysis of tropospheric sulfate aerosol and ozone for the period 1980-2005 using the aerosol-chemistry-climate model ECHAM5-HAMMOZ, Atmos. Chem. Phys., 11, 9563–9594, doi:10.5194/acp-11-9563-2011, 2011.

Pun, B. K. and Seigneur, C.: Investigative modeling of new pathways for secondary organic aerosol formation, Atmos. Chem. Phys., 7, 2199–2216, doi:10.5194/acp-7-2199-2007, 2007.

Pun, B. K., Griffin, R. J., Seigneur, C., and Seinfeld, J. H.: Secondary organic aerosol. 2. Thermodynamic model for gas/particle partitioning of molecular constituents, J. Geophys. Res., 107, 433, doi:10.1029/2001JD000542, 2002.

Pye, H. O. T. and Seinfeld, J. H.: A global perspective on aerosol from low-volatility organic compounds, Atmos. Chem. Phys., 10, 4377–4401, doi:10.5194/acp-10-4377-2010, 2010.

Geoscientific
Model Development
Discussions

Robinson, A. L., Donahue, N. M., Shrivastava, M. K., Weitkamp, E. A., Sage, A. M., Grieshop, A. P., Lane, T. E., Pierce, J. R., and Pandis, S. N.: Rethinking Organic Aerosols: Semivolatile Emissions and Photochemical Aging, Science, 315, 1259–1262, doi:10.1126/science.1133061, 2007.

S., Z., K., S., Y., Z., and A., N.: Three-dimensional modelling of the mixing state of particles over Greater Paris, J. Geophys. Res. Atmos., 121, 5930–5947, doi:10.1002/2015JD024241, 2016.

Sartelet, K., Debry, E., Fahey, K., Roustan, Y., Tombette, M., and Sportisse, B.: Simulation of aerosols and gas-phase species over Europe with the Polyphemus system. Part I: model-to-data comparison for 2001, Atmos. Environ., 41, 6116–6131, doi:10.1016/j.atmosenv.2007.04.024, 2007.

Sarwar, G., Luecken, D., Yarwood, G., Whitten, G. Z., and Carter, W. P. L.: Impact of an Updated Carbon Bond Mechanism on Predictions from the CMAQ Modeling System: Preliminary Assessment, J. Appl. Meteor. Climatol., 47, 3–14, doi:10.1175/2007JAMC1393.1, 2008.

Sarwar, G., Godowitch, J., Henderson, B. H., Fahey, K., Pouliot, G., Hutzell, W. T., Mathur, R., Kang, D., Goliff, W. S., and Stockwell, W. R.: A comparison of atmospheric composition using the Carbon Bond and Regional Atmospheric Chemistry Mechanisms, Atmos. Che. Phys., 13, 9695–9712, doi:10.5194/acp-13-9695-2013, 2013.

Seinfeld, J. H. and Pandis, S. N.: Atmospheric Chemistry and Physics, Wiley-interscience, 1998.

Semmler, M., Luo, B. P., and Koop, T.: Densities of liquid $H^+/NH_4^+/SO_4^{2-}/NO_3^-/H_2O$ solutions at tropospheric temperatures, Atmos. Environ., 40, 467–483, doi:10.1016/j.atmosenv.2005.09.056, 2006.

Shiraiwa, M. and Seinfeld, J. H.: Equilibration timescale of atmospheric secondary organic aerosol partitioning, Geophys. Res. Lett., 39, L24 801, doi:10.1029/2012GL054008, 2012.

Shiraiwa, M., Ammann, M., Koop, T., and Pöschl, U.: Gas uptake and chemical aging of semisolid organic aerosol particles, Proc. Natl. Acad. Sci., 108, 11 003–11 008, doi:10.1073/pnas.1103045108, 2011.

Skjøth, C. A., Geels, C., Berge, H., Gyldenkærne, S., Fagerli, H., Ellermann, T., Frohn, L. M., Christensen, J., Hansen, K. M., Hansen, K., and Hertel, O.: Spatial and temporal variations in ammonia emissions – a freely accessible model code for Europe, Atmos. Chem. and Phys., 11, 5221–5236, doi:10.5194/acp-11-5221-2011, 2011.

Solazzo, E., Bianconi, R., Pirovano, G., Matthias, V., Vautard, R., Moran, M. D., Appel, K. W., Bessagnet, B., Brandt, J., Christensen, J. H., Chemel, C., Coll, I., Ferreira, J., Forkel, R., Francis, X. V., Grell, G., Grossi, P., Hansen, A. B., Miranda, A. I., Nopmongcol, U., Prank, M., Sartelet, K. N., Schaap, M., Silver, J. D., Sokhi, R. S., Vira, J., Werhahn, J., Wolke, R., Yarwood, G., Zhang, J., Rao, S. T., and Galmarini, S.: Operational model evaluation for particulate matter in Europe and North America in the context of AQMEII, Atmos. Environ., 53, 75–92, doi:10.1016/j.atmosenv.2012.02.045, 2012.

Surratt, J. D., Chan, A. W. H., Eddingsaas, N. C., Chan, M. N., Loza, C. L., Kwan, A. J., Hersery, S. P., Flagan, R. C., Wennberg, P. O., and Seinfeld, J. H.: Reactive intermediates revealed in secondary organic aerosol formation from isoprene, Proc. Natl. Acad. Sci., 107, 6640–6645, doi:10.1073/pnas.0911114107, 2010.

Tørseth, K., Aas, W., Breivik, K., Fjaeraa, A. M., Fiebig, M., Hjellbrekke, A. G., Lund Myhre, C., Solberg, S., and Yttri, K. E.: Introduction to the European Monitoring and Evaluation Programme (EMEP) and observed atmospheric composition change during 1972–2009, Atmos. Chem. Phys., 12, 5447–5481, doi:10.5194/acp-12-5447-2012, 2012.

Tsyro, S., Aas, W., Soares, J., Sofiev, M., Berge, H., and Spindler, G.: Modelling of sea salt concentrations over Europe: key uncertainties and comparison with observations, Atmos. Chem. Phys., 11, 10 367–10 388, doi:10.5194/acp-11-10367-2011, 2011.

Turpin, B. J. and Lim, H.-J.: Species contributions to $PM_{2.5}$ mass concentrations: revisiting common assumptions for estimating organic mass, Aerosol. Sci. Tech., 35, 602–610, doi:10.1080/02786820119445, 2001.

Vaden, T. D., Imre, D., Berankek, J., Shrivastava, M., and Zelenyuk, A.: Evaporation kinetics and phase of laboratory and ambient secondary organic aerosol, Proc. Natl. Acad. Sci., 108, 2190–2195, doi:10.1073/pnas.1013391108, 2011.

Vestreng, V.: Review and revision. Emission data reported to CLRTAP Tech. Rep., EMEP MSW-W, Tech. rep., Norwegian Meteorological Institute, Oslo, Norway, 2003.

5 Virtanen, A., Joutsensaari, J., Koop, T., Kannosto, J., YliPirilä, P., Leskinen, J., Mäkelä, J. M., Holopainen, J. K., Pöschl, U., Kulmala, M., Worsnop, D. R., and Laaksonen, A.: An amorphous solid state of biogenic secondary organic aerosol particles, Nature, 467, 824–827, doi:10.1038/nature09455, 2010.

Wesely, M.: Parameterization of Surface Resistances to Gaseous Dry Deposition in Regional-Scale Numerical Models, Atmos. Environ., 23, 1293–1304, doi:10.1016/0004-6981(89)90153-4, 1989.

10 Yu, S., Bhave, P. V., Dennis, R. L., and Marthur, R.: Seasonal and regional variations of primary and secondary organic aerosols over the Continental United States: Semi-empirical estimates and model evaluation, Environ. Sci. Technol., 41, 4690–4697, doi:10.1021/es061535g, 2007.

Yuan, H., Dai, Y., Xiao, Z., Ji, D., and Shangguan, W.: Reprocessing the MODIS Leaf Area Index Products for Land Surface and Climate Modelling, Remote Sensing of Environment, 155, 1171–1187, doi:10.1016/j.rse.2011.01.001, 2011.

15 Zhang, Q., Jimenez, J. L., Canagaratna, M. R., Allan, J. D., Coe, H., Ulbrich, I., Alfarra, M. R., Takami, A., Middlebrook, A. M., Sun, Y. L., Dzepina, K., Dunlea, E., Docherty, K., De-Carlo, P. F., Salcedo, D., Onasch, T., Jayne, J. T., Miyoshi, T., Shimono, A., Hatakeyama, S., Takegawa, N., Kondo, Y., Schneider, J., Drewnick, F., Borrmann, S., Weimer, S., Demerjian, K., Williams, P., Bower, K., Bahreini, R., Cottrell, L., Griffin, R. J., Rautiainen, J., Sun, J. Y., Zhang, Y. M., and Worsnop, D. R.: Ubiquity and dominance of oxygenated species in organic aerosols in anthropogenically-influence Northern Hemisphere mildlatitudes, Geophys. Res. Lett., 34, L13 801, 20 doi:10.1029/2007GL029979, 2007.

Zhang, Y., Pan, Y., Wang, K., Fast, J. D., and Grell, G. A.: WRF/Chem-MADRID: Incorporation of an aerosol module into WRF/Chem and its initial application to the TexAQS2000 episode, J. Geophys. Res., 115, D18 202, doi:10.1029/2009JD013443, 2010.

Zhao, B., Wang, S., Donahue, N. M., Jathar, S. H., Huang, X., Wu, W., Hao, J., and Robinson, A. L.: Quantifying the effect of organic aerosol aging and intermediate-volatility emissions on regional-scale aerosol pollution in China, Sci. Rep., 6, 28 815, doi:10.1038/srep28815, 25 2016a.

Zhao, Y., Nguyen, N. T., Presto, A. A. Hennigan, C. J., May, A. A., and Robinson, A. L.: Intermediate Volatility Organic Compound Emissions from On-Road Gasoline Vehicles and Small Off-Road Gasoline Engines, Environ. Sci. Technol., 50, 4554–5463, doi:10.1021/acs.est.5b06247, 2016b.

Zhu, S., Sartelet, K., and Seigneur, C.: A size-composition resolved aerosol model for simulating the dynamics of externally mixed particles: 30 SCRAM (v 1.0), Geosci. Model Dev., 8, 1595–1612, doi:10.5194/gmd-8-1595-2015, 2015.

Zhu, S., Sartelet, K., R., H., and J., W.: Simulation of particle diversity and mixing state over Greater Paris: A model-measurement intercomparison, Faraday Discuss., 189, 547–566, doi:10.1039/C5FD00175G, 2016.

Zuend, A. and Seinfeld, J. H.: Modeling the gas-particle partitioning of secondary organic aerosol: the importance of liquid-liquid phase separation, Atmos. Chem. Phys., 12, 3857–3882, doi:10.5194/acp-12-3857-2012, 2012.

35 Zuend, A., Marcolli, C., Luo, B. P., and Peter, T.: A thermodynamic model of mixed organic-inorganic aerosols to predict activity coefficients, Atmos. Chem. Phys., 8, 4559–4593, doi:10.5194/acp-8-4559-2008, 2008.

Zuend, A., Marcolli, C., Booth, A. M., Lienhard, D. M., Soonsin, V., Krieger, U. K., Topping, D. O., McFiggans, G., Peter, T., and Seinfeld, J. H.: New and extended parameterization of the thermodynamic model AIOMFAC: calculation of activity coefficients for organic-

inorganic mixtures containing carboxyl, hydroxyl, carbonyl, ether, ester, alkenyl, alkyl, and aromatic functional groups, Atmos. Chem. Phys., 11, 9155–9206, doi:10.5194/acp-11-9155-2011, 2011.
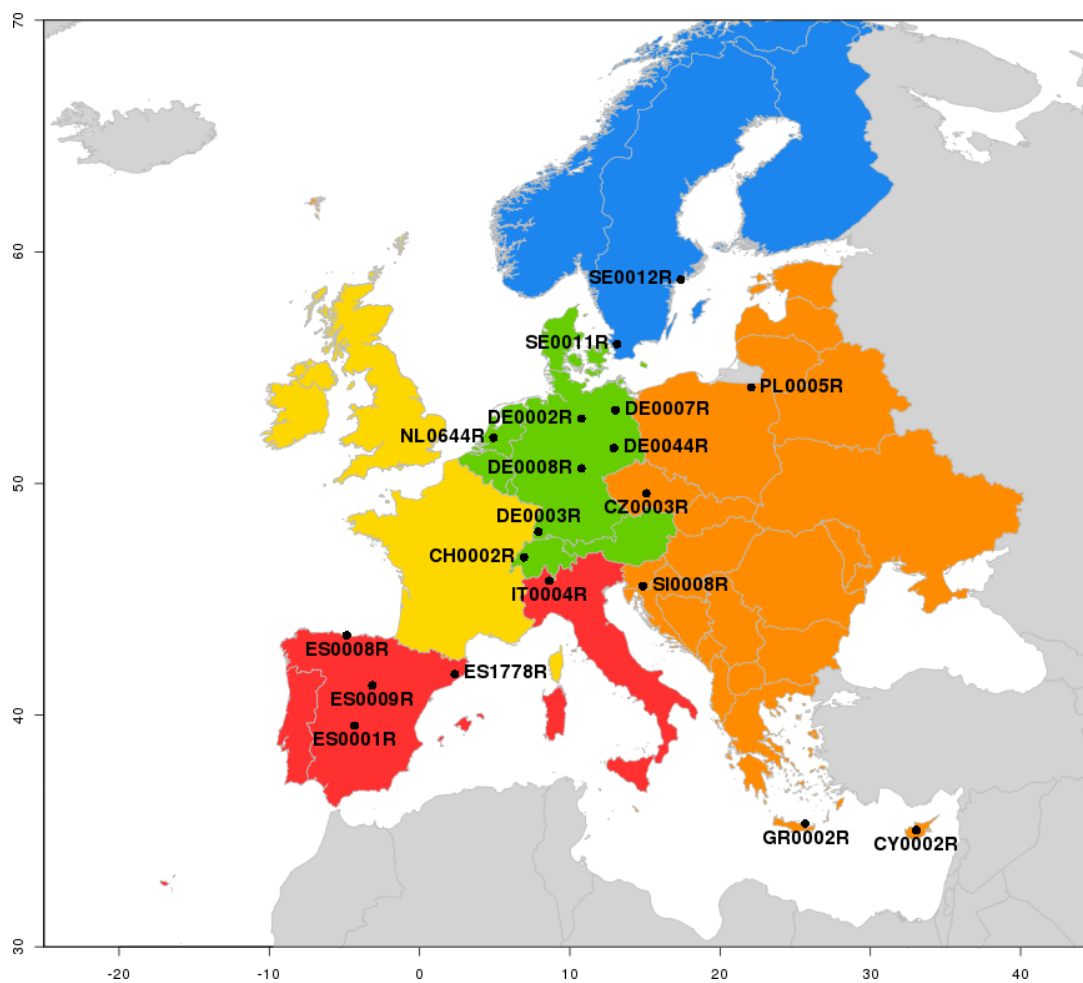
Geoscientific
Model Development
Discussions

Figure 1. Maps of regions defined in this study and of mentionned stations. The chosen regions are: Southern Europe (Red), Western Europe (Yellow), Central Europe (Green), Eastern Europe (Orange), Northern Europe (Blue).

Table 1. Reactions leading to SOA formation[a].

Reaction	Kinetic rate parameter
	(s^{-1} or molecule^{-1}.cm^3.s^{-1})
ISOP + OH → ISOR + OH	$2.54 \times 10^{-11} \times \exp(\frac{408}{T})$
ISOP + NO$_3$ → ISON + NO$_3$	$3.03 \times 10^{-12} \times \exp(\frac{-448}{T})$
ISOR + HO$_2$ → 0.282 BiPER + 0.030 BiDER + HO$_2$	$2.05 \times 10^{-13} \times \exp(\frac{1300}{T})$
ISOR + C$_2$O$_3$ → 0.026 BiMT + 0.219 MACR + C$_2$O$_3$	$8.40 \times 10^{-14} \times \exp(\frac{221}{T})$
ISOR + MeO$_2$ → 0.026 BiMT + 0.219 MACR + MeO$_2$	$3.40 \times 10^{-14} \times \exp(\frac{221}{T})$
ISOR + NO → 0.418 MACR + 0.046 ISON + NO	$2.43 \times 10^{-12} \times \exp(\frac{360}{T})$
ISOR + NO$_3$ → 0.438 MACR + NO$_3$	1.20×10^{-12}
ISON + OH → OH	1.30×10^{-11}
ISON + NO$_3$ → 0.074 BiNIT3 + NO$_3$	6.61×10^{-13}
MACR + NO → NO	$2.54 \times 10^{-12} \times \exp(\frac{360}{T})$
MACR + HO$_2$ → HO$_2$	$1.82 \times 10^{-13} \times \exp(\frac{1300}{T})$
MACR + MeO$_2$ → MeO$_2$	$3.40 \times 10^{-14} \times \exp(\frac{221}{T})$
MACR + NO$_2$ → MPAN + NO$_2$	$2.80 \times 10^{-12} \times \exp(\frac{181}{T})$
MPAN → MACR	$1.60 \times 10^{16} \times \exp(\frac{-13486}{T})$
MPAN + OH → 0.067 BiMGA + 0.047 BiNGA + OH	3.20×10^{-11}
MPAN + NO$_3$ → 0.067 BiMGA + 0.047 BiNGA + NO$_3$	3.20×10^{-11}
BiPER + hν → Degradation products	k = 50 × kinetic of photolysis of H$_2$O$_2$

Geoscientific
Model Development
Discussions

Open Access

Reaction	Kinetic rate parameter
	(s^{-1} or $molecule^{-1}.cm^3.s^{-1}$)
API + OH → 0.30 BiA0D + 0.17 BiA1D + 0.10 BiA2D + OH	$1.21 \times 10^{-11} \times \exp(\frac{440}{T})$
API + O$_3$ → 0.18 BiA0D + 0.16 BiA1D + 0.05 BiA2D + O$_3$	$5.00 \times 10^{-16} \times \exp(\frac{-530}{T})$
API + NO$_3$ → 0.70 BiA0D + 0.10 BiNIT + NO$_3$	$1.19 \times 10^{-12} \times \exp(\frac{-490}{T})$
BPI + OH → 0.07 BiA0D + 0.08 BiA1D + 0.06 BiA2D + OH	$2.38 \times 10^{-11} \times \exp(\frac{357}{T})$
BPI + O$_3$ → 0.09 BiA0D + 0.13 BiA1D + 0.04 BiA2D + O$_3$	1.50×10^{-17}
BPI + NO$_3$ → 0.02 BiA0D + 0.63 BiNIT + NO$_3$	2.51×10^{-12}
LIM + OH → 0.35 BiA0D + 0.20 BiA1D + 0.0035 BiA2D + OH	$4.20 \times 10^{-11} \times \exp(\frac{401}{T})$
LIM + O$_3$ → 0.09 BiA0D + 0.10 BiA1D + O$_3$	$2.95 \times 10^{-15} \times \exp(\frac{783}{T})$
LIM + NO$_3$ → 0.69 BiA0D + 0.27 BiNIT + NO$_3$	1.22×10^{-11}
HUM + OH → 0.74 BiBmP + 0.26 BiBlP + OH	2.93×10^{-10}
TOL + OH → ... + 0.25 TOLP	$1.80 \times 10^{-12} \times \exp(\frac{355}{T})$
TOLP + HO$_2$ → 0.78 AnClP + HO$_2$	$3.75 \times 10^{-13} \times \exp(\frac{980}{T})$
TOLP + C$_2$O$_3$ → 0.78 AnClP + C$_2$O$_3$	$7.40 \times 10^{-13} \times \exp(\frac{765}{T})$
TOLP + MeO$_2$ → 0.78 AnClP + MeO$_2$	$3.56 \times 10^{-14} \times \exp(\frac{708}{T})$
TOLP + NO → 0.097 AnBlP + 0.748 AnBmP + NO	$2.70 \times 10^{-12} \times \exp(\frac{360}{T})$
TOLP + NO$_3$ → 0.097 AnBlP + 0.748 AnBmP + NO$_3$	1.2×10^{-12}
XYL + OH → ... + 0.274 XYLP	$1.70 \times 10^{-11} \times \exp(\frac{116}{T})$
XYLP + HO$_2$ → 0.71 AnClP + HO$_2$	$3.75 \times 10^{-13} \times \exp(\frac{980}{T})$
XYLP + C$_2$O$_3$ → 0.71 AnClP + C$_2$O$_3$	$7.40 \times 10^{-13} \times \exp(\frac{765}{T})$
XYLP + MeO$_2$ → 0.71 AnClP + MeO$_2$	$3.56 \times 10^{-14} \times \exp(\frac{708}{T})$
XYLP + NO → 0.063 AnBlP + 0.424 AnBmP + NO	$2.70 \times 10^{-12} \times \exp(\frac{360}{T})$
XYLP + NO$_3$ → 0.063 AnBlP + 0.424 AnBmP + NO$_3$	1.2×10^{-12}

[a] Oxidants may be present as both reactants and products so that a reaction added to CB05 will not affect the original photochemical oxidant concentrations.

**Geoscientific
Model Development
Discussions**

Table 2. Properties of the surrogate SOA species.

Surrogate	Type [a]	H [b]	P^{0} [c]	ΔH_{vap} [d]	Comments
BiMT	hydrophilic	0.805	1.45×10^{-6}	38.4	-
BiPER	hydrophilic	0.111	2.61×10^{-6}	38.4	-
BiDER	hydrohilic	2.80	4.10×10^{-7}	38.4	-
BiMGA	hydrophilic	1.13×10^{-2}	1.4×10^{-5}	43.2	$pK_a = 4.0$
BiNGA	hydrophobic	-	1.4×10^{-5}	43.2	$K_{p,eff} = K_p(1 + K_{oligo})$ [e]
BiNIT3	hydrophobic	-	1.45×10^{-6}	38.4	-
BiA0D	hydrophilic	4.82×10^{-5}	2.70×10^{-4}	50	See Eq. 4
BiA1D	hydrophilic	2.73×10^{-3}	2.17×10^{-7}	50	$pK_a = 3.2$
BiA2D	hydrophilic	6.52×10^{-3}	1.43×10^{-7}	50	$pK_{a1} = 3.4$, $pK_{a2} = 5.1$
BiNIT	hydrophobic	-	2.5×10^{-6}	109	-
BiBlP	hydrophobic	-	6.0×10^{-10}	175	-
BiBmP	hydrophobic	-	3.0×10^{-7}	175	-
AnBlP	hydrophobic	-	6.8×10^{-8}	50	-
AnBmP	hydrophobic	-	8.4×10^{-6}	50	-
AnClP	hydrophobic	-	-	non volatile	-

[a] Type A: hydrophilic species, type B: hydrophobic species, type C: hydrophobic non-volatile species, which is not used to compute activity coefficients

[b] Henry's law constant [$(\mu g/\mu g$ water$)/(\mu g/m^3)$]

[c] Saturation vapor pressure [torr]

[d] Enthalpy of vaporization [kJ.mol^{-1}]

[e] K_{oligo} (equal to 64.2) is used to take into account the formation of oligomers (Couvidat et al., 2012). $K_{p,eff}$ is the effective partitioning constant and K_p is the partitioning constant calculated as in Pankow (1994).

Table 3. Properties of primary and aged SVOC.

Surrogate	MW[a]	K_p [b]	ΔH_{vap} [c]
POAlP	280	1.1	106
POAmP	280	0.0116	91
POAhP	280	0.00031	79
SOAlP	392	110	106
SOAmP	392	1.16	91
SOAhP	392	0.031	79

[a] Molecular weight [g.mol^{-1}]

[b] Partitioning constant [m^3.μg^{-1}]

[c] Enthalpy of vaporization [kJ.mol^{-1}]
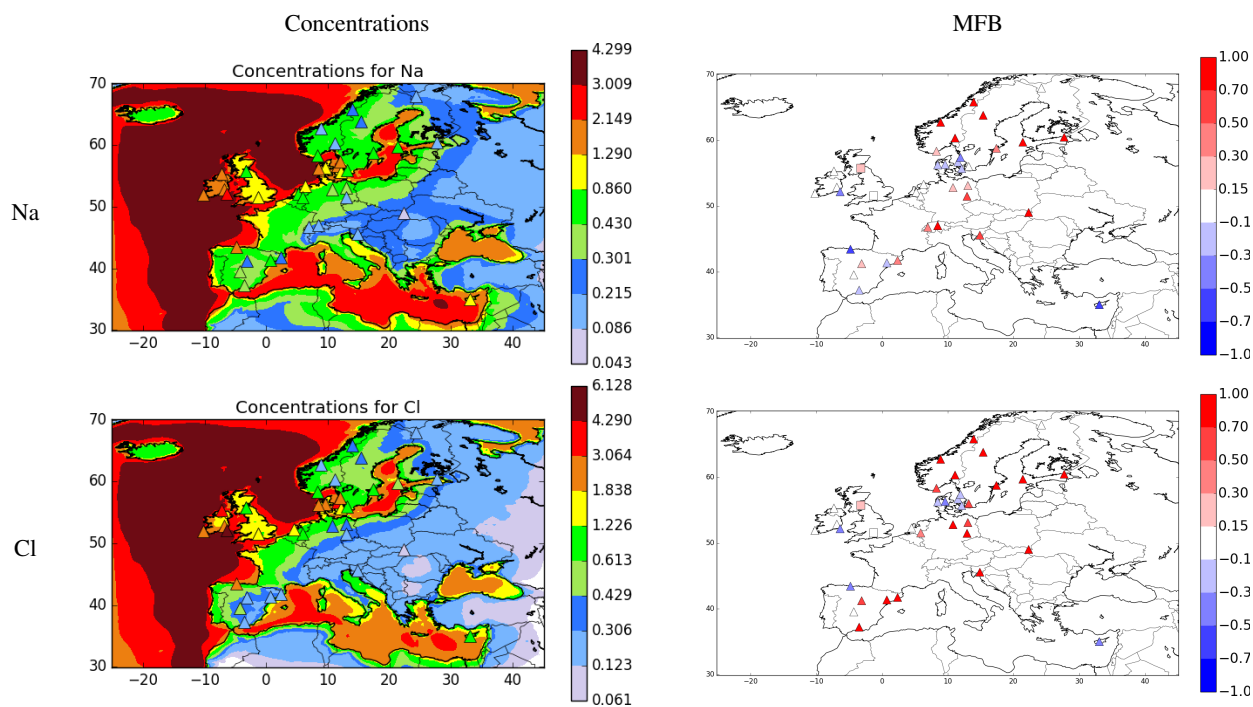
Figure 2. Modeled concentrations (in μg m^{-3}) and MFB for Na and Cl in 2013. Triangles correspond to measured concentrations in the left and to the MFB value in the right.

Table 4. Effective Henry's law constant used for dry and wet deposition.

Compound	H (mol/L/atm)
O_3	0.01
SO_2	10^5
NO_2	0.01
NO	2×10^{-3}
NH_3	10^5
BiA0D	1.8e6
BiA1D	2.92e10
BiA2D	4.23e10
BiMT	3.3e10
BiPER	8.09e9
BiDER	8.91e10
BiMGA	2.15e10
AnBlP	0.01
AnBmP	0.01
BiBlP	1.17e8
BiBmP	3.05e5
AnClP	0.01
BiNGA	2.71e9
BiNIT3	4.75e6
BiNIT	7.66e4
POAlP	0.01
POAmP	0.01
POAhP	0.01
SOAlP	3000
SOAmP	3000
SOAhP	3000

Table 5. Annual statistics for the comparison of daily concentrations. Means and RMSE are in μg m^{-3}.

	O3	NO$_2$	PM$_{10}$	PM$_{2.5}$	NO$_3$	NH$_4$	SO$_4$	Na	Cl	TNO$_3$	TNH$_4$
Number of stations	117	81	59	41	37	33	56	38	35	42	42
Model mean	71.78	6.83	14.42	10.54	1.99	1.29	1.66	0.67	1.28	2.55	2.16
Measurement mean	63.90	6.57	13.51	9.06	1.46	0.89	1.6	0.69	1.17	2.07	1.49
RMSE	19.62	6.4	9.34	6.95	1.87	0.97	1.13	0.76	1.49	2.0	2.0
Correlation	0.62	0.6	0.6	0.68	0.71	0.71	0.67	0.66	0.67	0.69	0.56
MFB	0.02	-0.03	0.08	0.22	0.15	0.36	0.13	0.06	0.09	0.10	0.20
MFE	0.16	0.51	0.44	0.48	0.57	0.55	0.44	0.52	0.49	0.50	0.55

Table 6. Comparison of modeled concentrations to measured concentrations of OC. Means and RMSE are in μg m^{-3}.

Station	Modeled mean	Measured mean	RMSE	correlation	MFB	MFE
CH0002R	2.48	3.29	1.70	0.67	-0.13	0.37
CY0002R	0.91	1.65	1.65	0.07	-0.35	0.65
CZ0003R	1.97	3.64	2.28	0.72	-0.63	0.67
DE0002R	1.20	2.40	1.79	0.40	-0.68	0.75
DE0003R	1.83	1.27	1.28	0.35	0.40	0.63
DE0007R	1.28	2.26	2.03	0.29	-0.56	0.73
DE0008R	1.49	1.73	1.18	0.49	-0.03	0.54
DE0044R	1.67	3.65	2.45	0.82	-0.74	0.76
ES0001R	0.90	1.79	1.18	0.64	-0.65	0.70
ES0009R	0.69	1.79	1.87	0.07	-0.77	0.87
ES1778R	1.97	1.60	1.07	0.68	0.36	0.48
IT0004R	10.4	6.36	7.43	0.84	0.40	0.55
NL0644R	1.21	2.57	1.53	0.84	-0.87	0.87
PL0005R	1.87	3.04	2.18	0.71	-0.42	0.49
SI0008R	4.70	4.19	2.45	0.53	-0.01	0.40
GR0002R	0.82	1.78	1.42	0.19	-0.65	0.72
SE0011R	0.84	1.14	0.71	0.41	-0.32	0.50
SE0012R	0.73	1.53	1.16	0.74	-0.70	0.72

Geoscientific
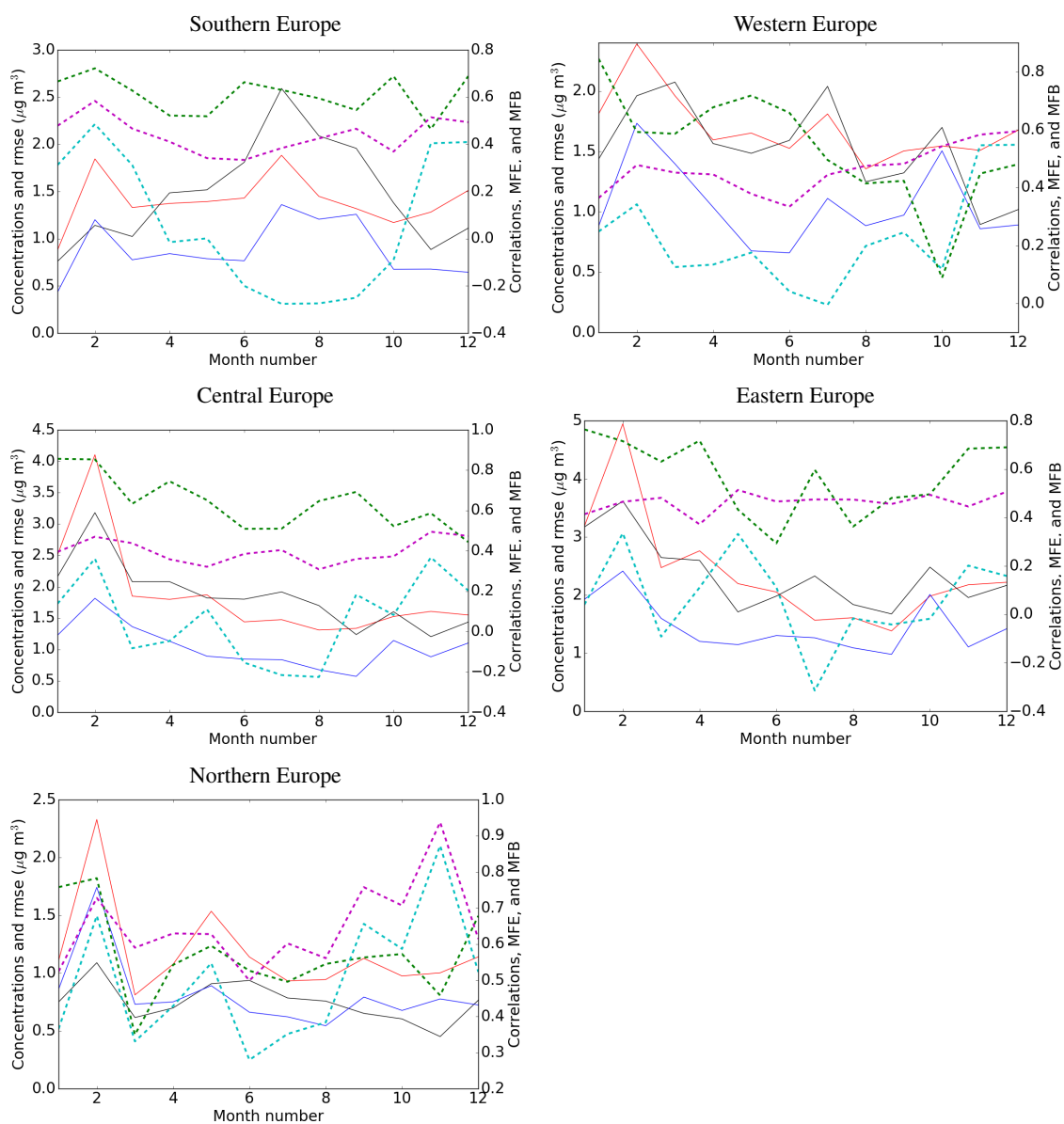Model Development
Discussions
Open Access
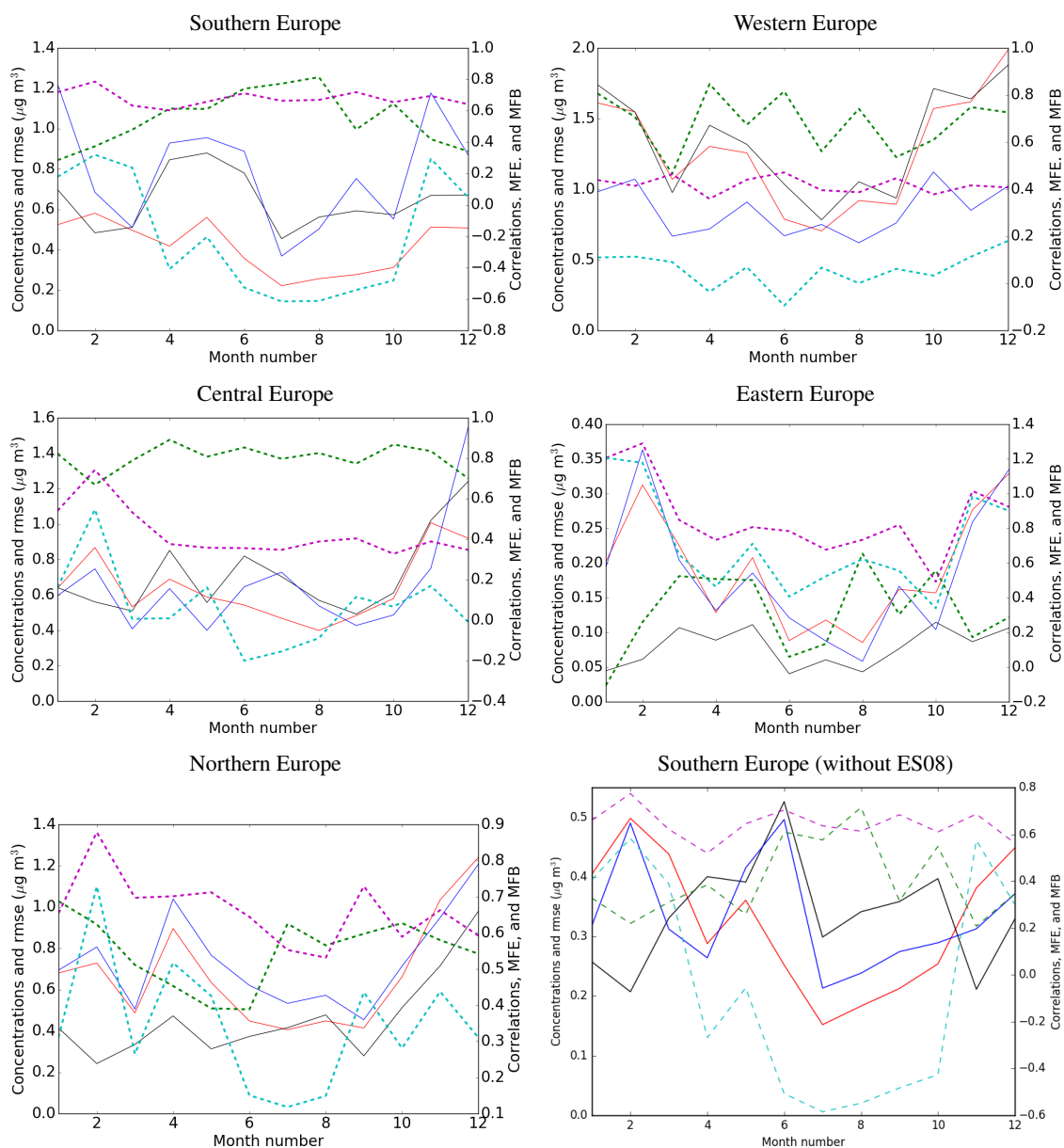
Figure 3. Seasonal evolution of statistics by regions for Na: Monthly mean measured concentrations (black), monthly mean modeled concentrations (red), monthly RMSE (blue), monthly spatiotemporal correlations (green), monyhly MFB (cyan) and monthly MFE (magenta). Solid curves refer to the left axis while dotted curves refer to the right axis.
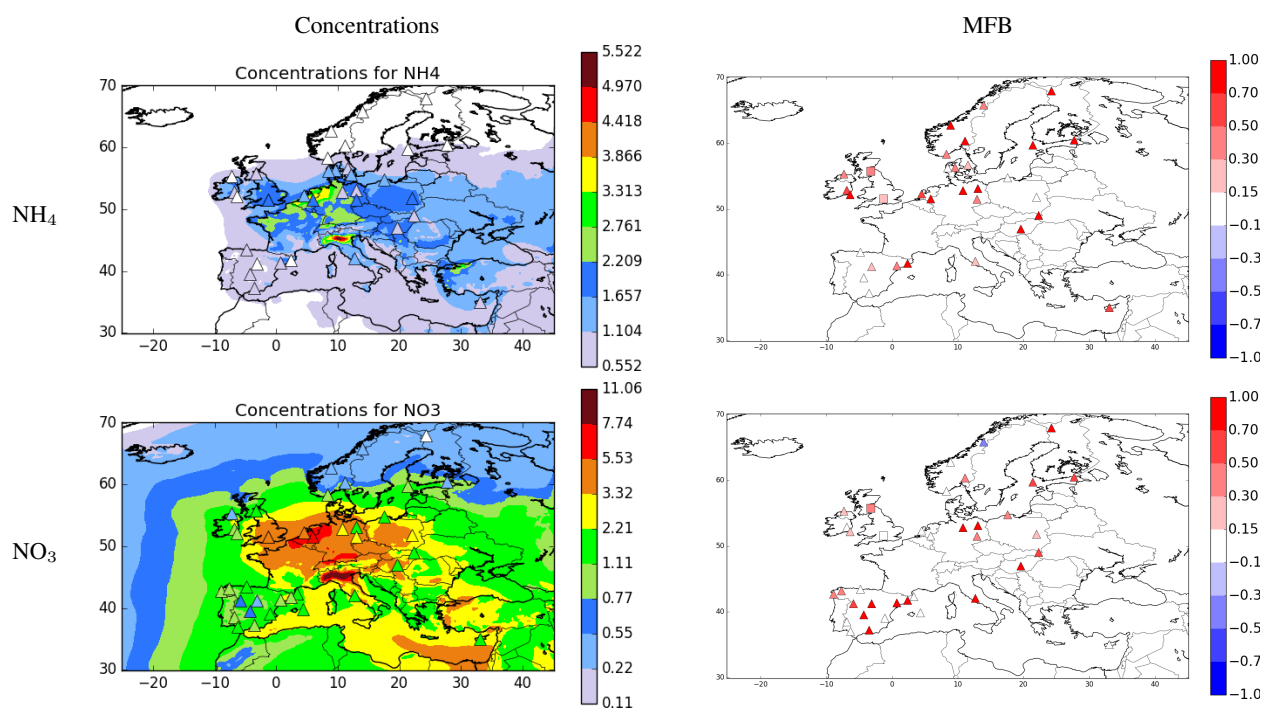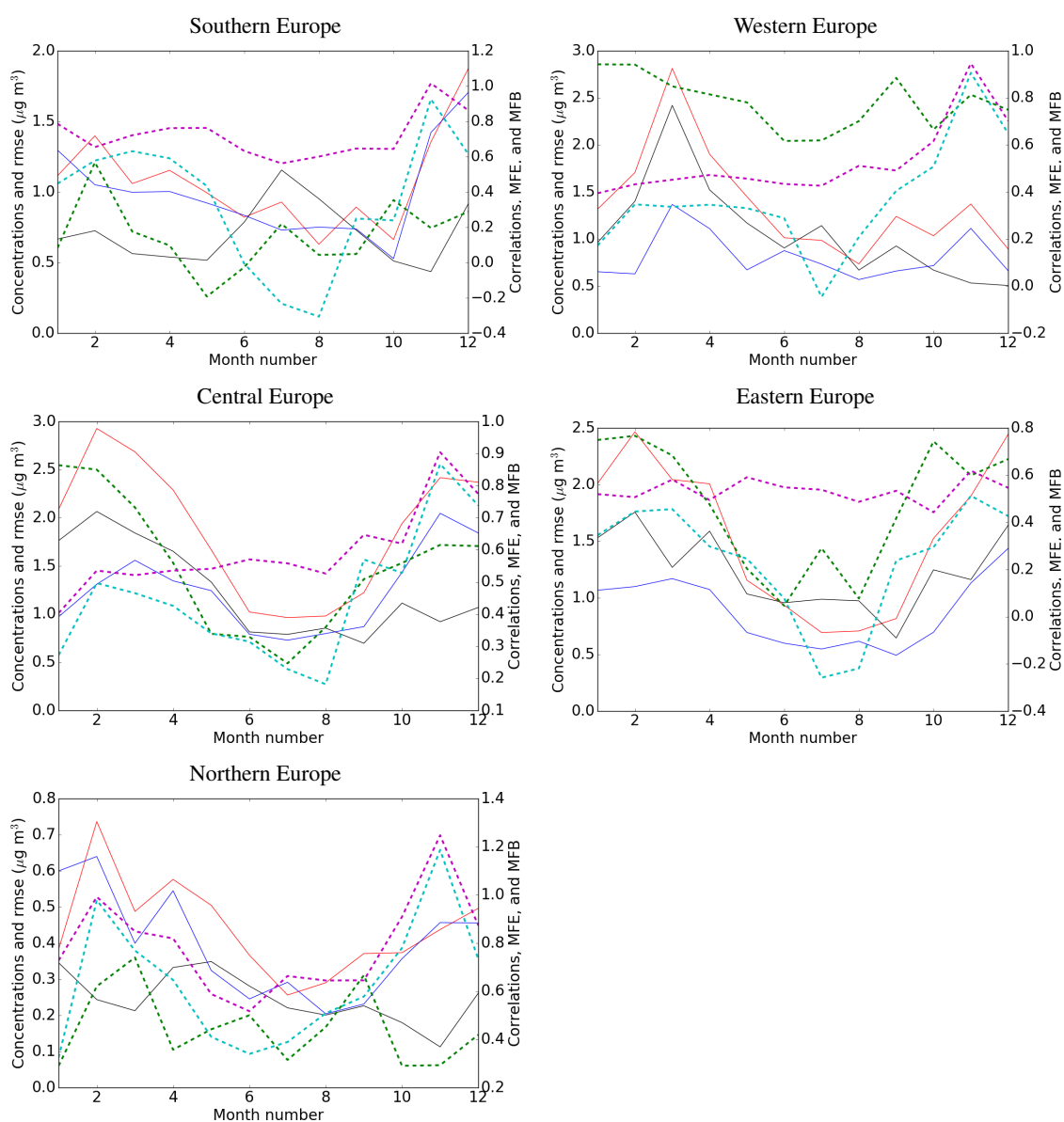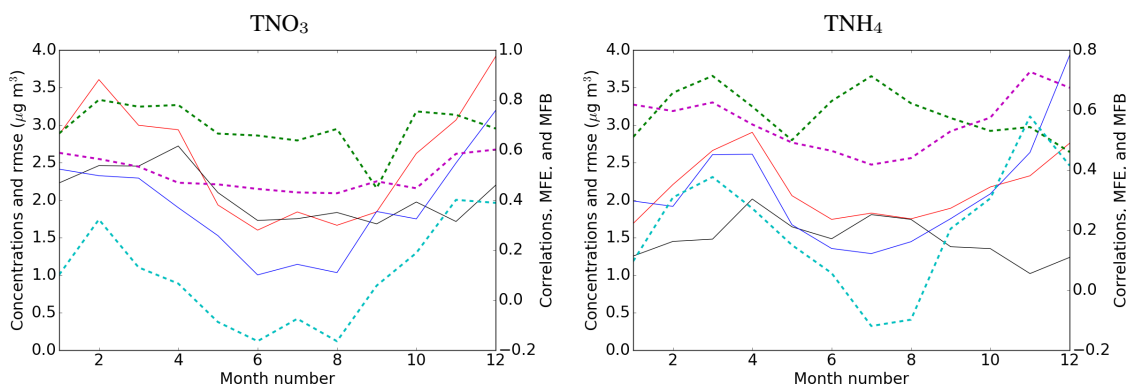
Geoscientific
Model Development
Discussions
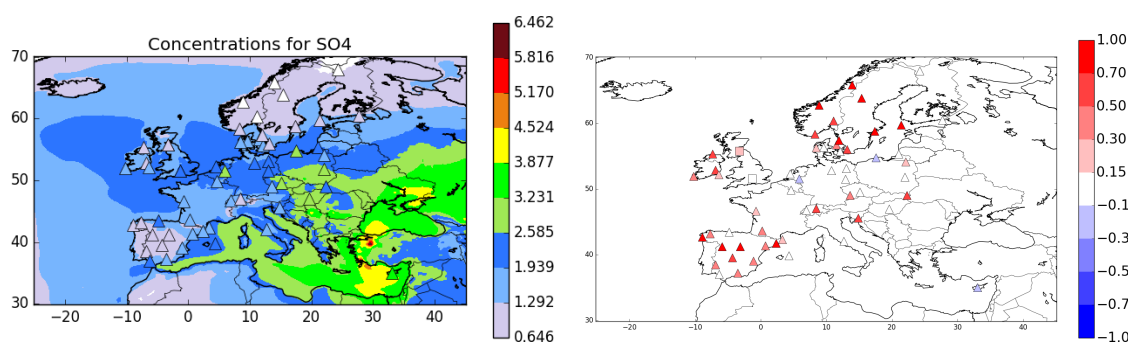
Figure 4. Modeled concentrations (in $\mu g\ m^{-3}$) and MFB for SO$_4$ in 2013. Triangles correspond to measured concentrations in the left and to the MFB value in the right.

Figure 5. Seasonal evolution of statistics by regions for SO_4: Monthly mean measured concentrations (black), monthly mean modeled concentrations (red), monthly RMSE (blue), monthly spatiotemporal correlations (green), monyhly MFB (cyan) and monthly MFE (magenta). Solid curves refer to the left axis while dotted curves refer to the right axis.

Geoscientific
Model Development
Discussions

Figure 6. Modeled concentrations (in μg m^{-3}) and MFB for NH$_4$ and NO$_3$ in 2013. Triangles correspond to measured concentrations in the left and to the MFB value in the right.
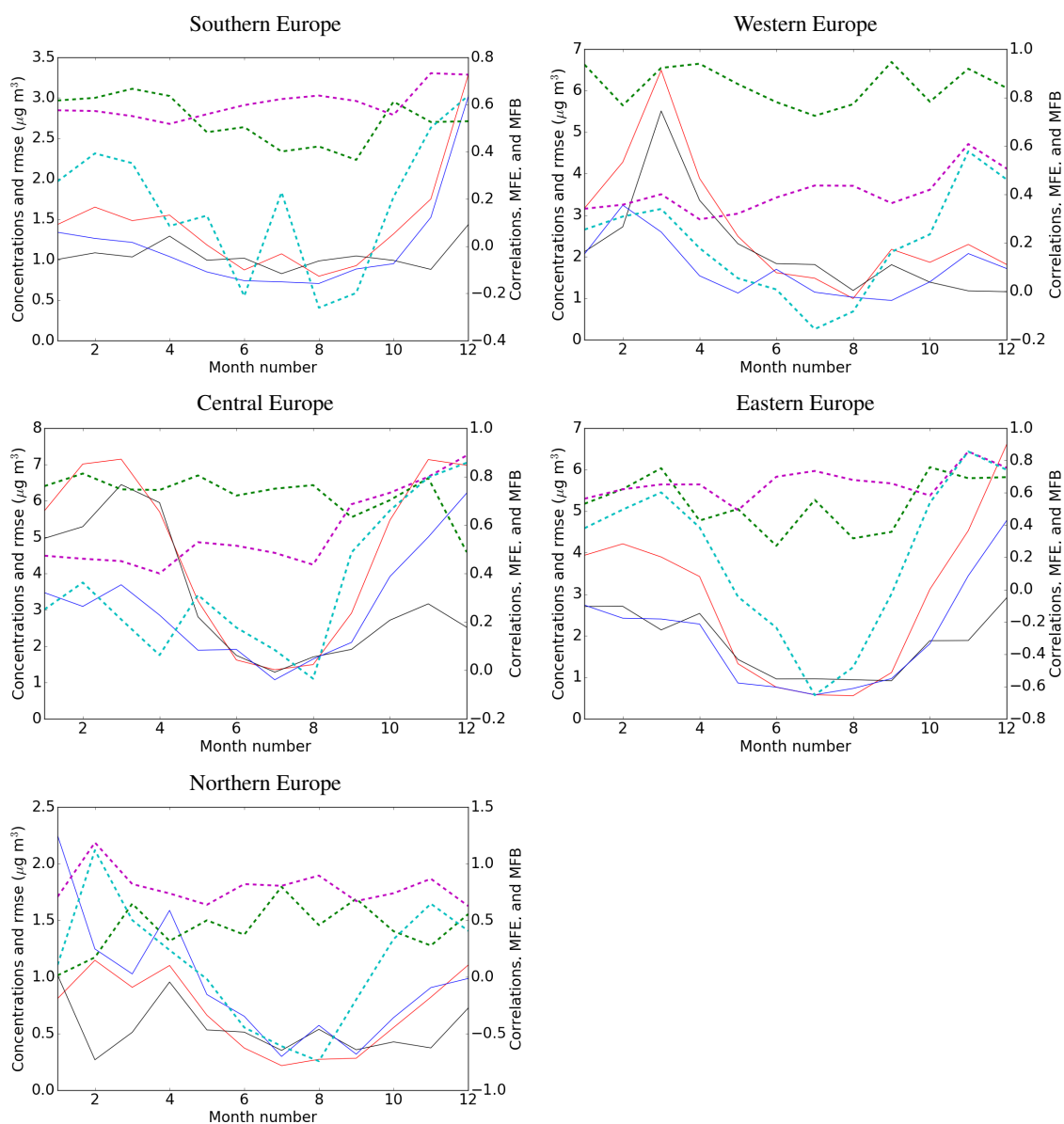
Figure 7. Seasonal evolution of statistics by regions for NO$_3$: Monthly mean measured concentrations (black), monthly mean modeled concentrations (red), monthly RMSE (blue), monthly spatiotemporal correlations (green), monyhly MFB (cyan) and monthly MFE (magenta). Solid curves refer to the left axis while dotted curves refer to the right axis.

Geoscientific
Model Development
Discussions

Figure 8. Seasonal evolution of statistics by regions for NH$_4$: Monthly mean measured concentrations (black), monthly mean modeled concentrations 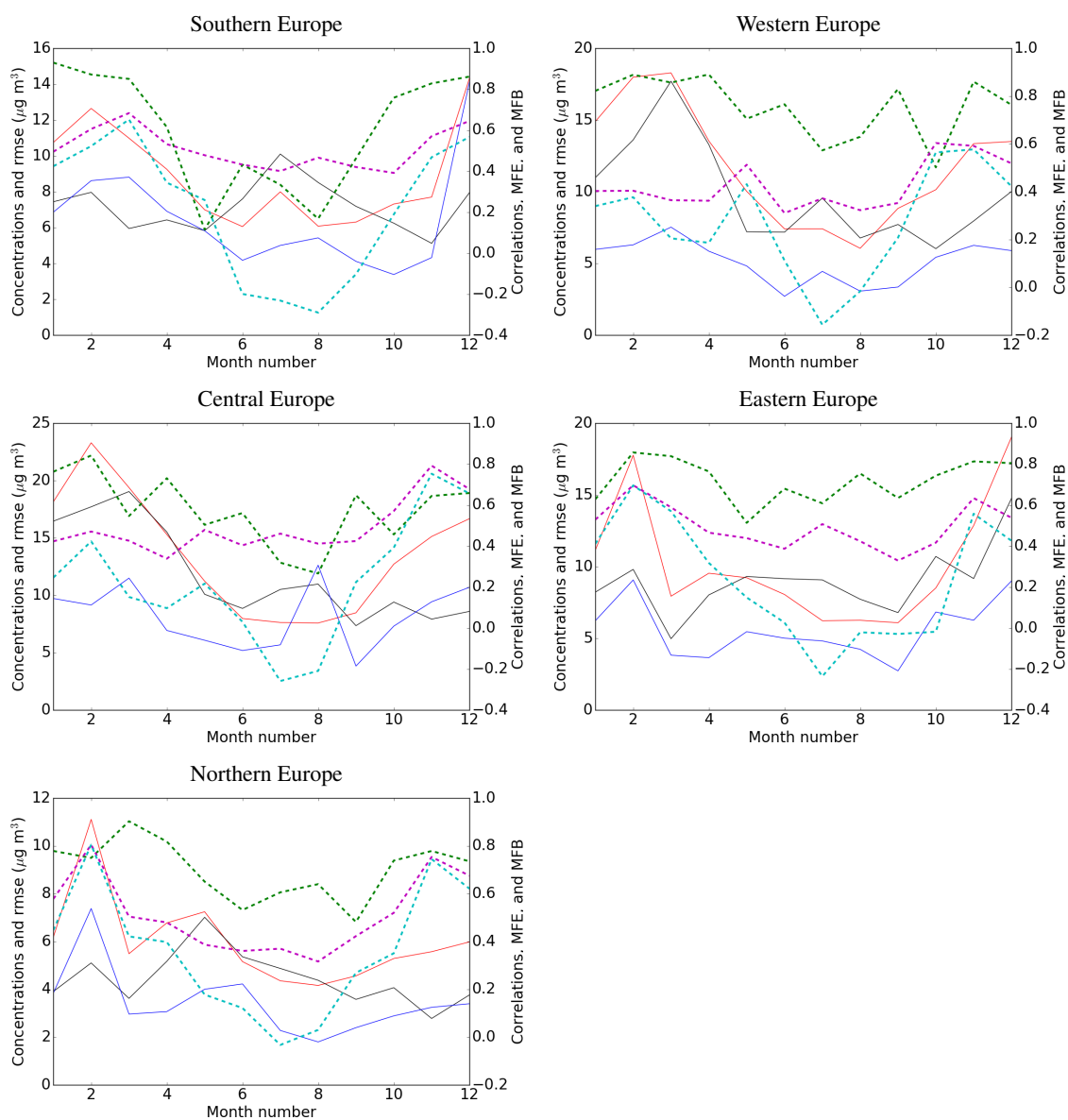(red), monthly RMSE (blue), monthly spatiotemporal correlations (green), monyhly MFB (cyan) and monthly MFE (magenta). Solid curves refer to the left axis while dotted curves refer to the right axis.

Geoscientific
Model Development
Discussions

Figure 9. Seasonal evolution of statistics for the all Europe for TNO$_3$ and TNH$_4$: Monthly mean measured concentrations (black), monthly mean modeled concentrations (red), monthly RMSE (blue), monthly spatiotemporal correlations (green), monthly MFB (cyan) and monthly MFE (magenta).
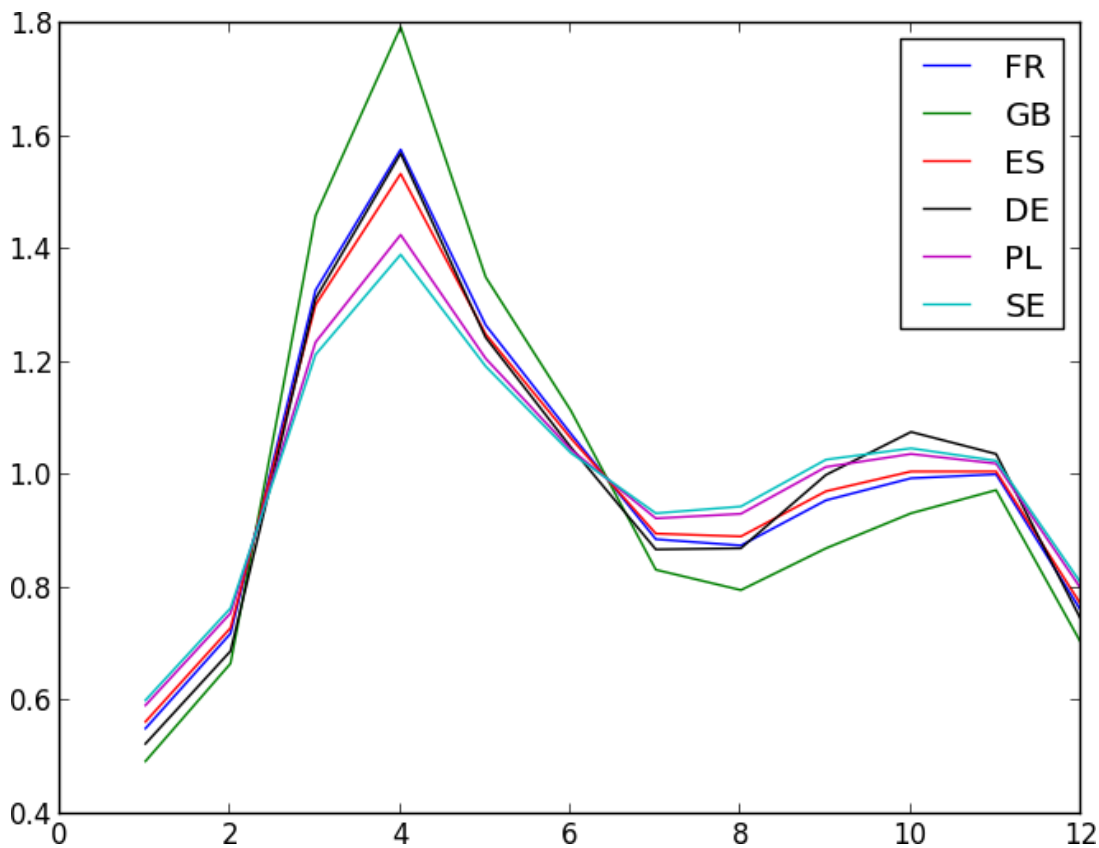
Figure 10. Seasonal evolution of NH$_3$ emissions used in CHIMERE for several countries.
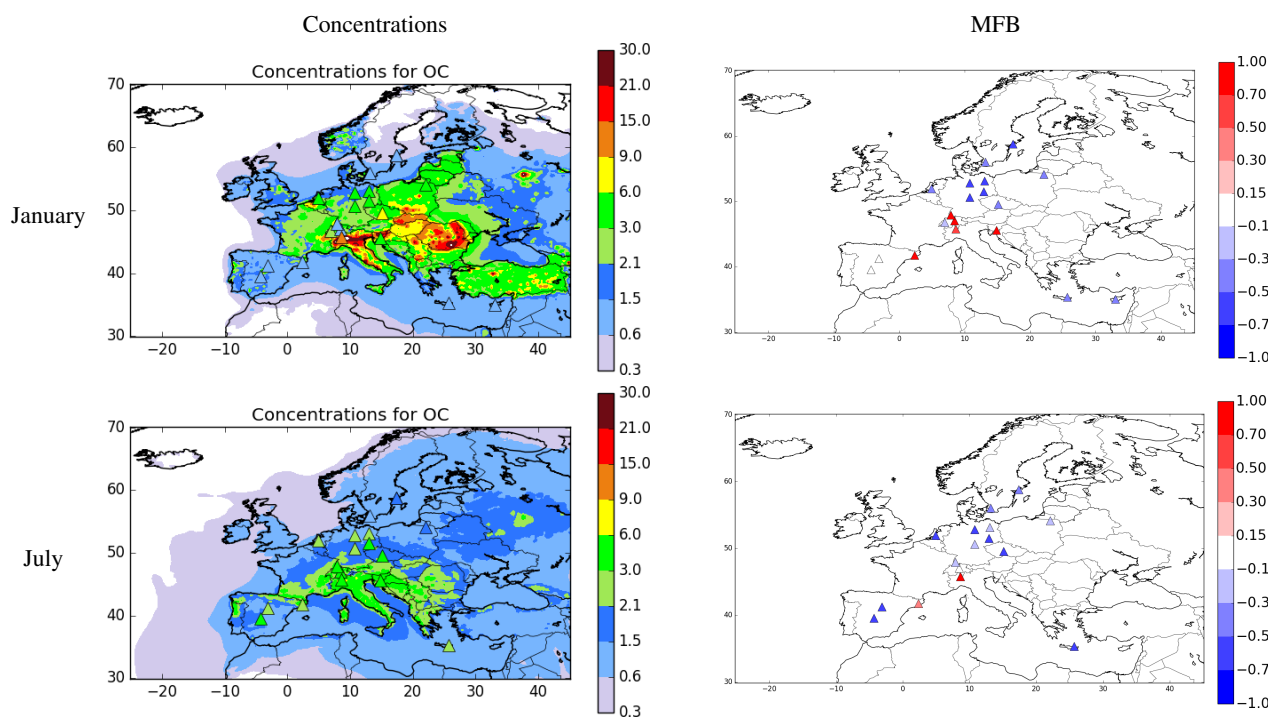
Figure 11. Modeled concentrations (in $\mu g\ m^{-3}$) and MFB for Organic Carbon in January and July 2013. Triangles correspond to measured concentrations in the left and to the MFB value in the right.
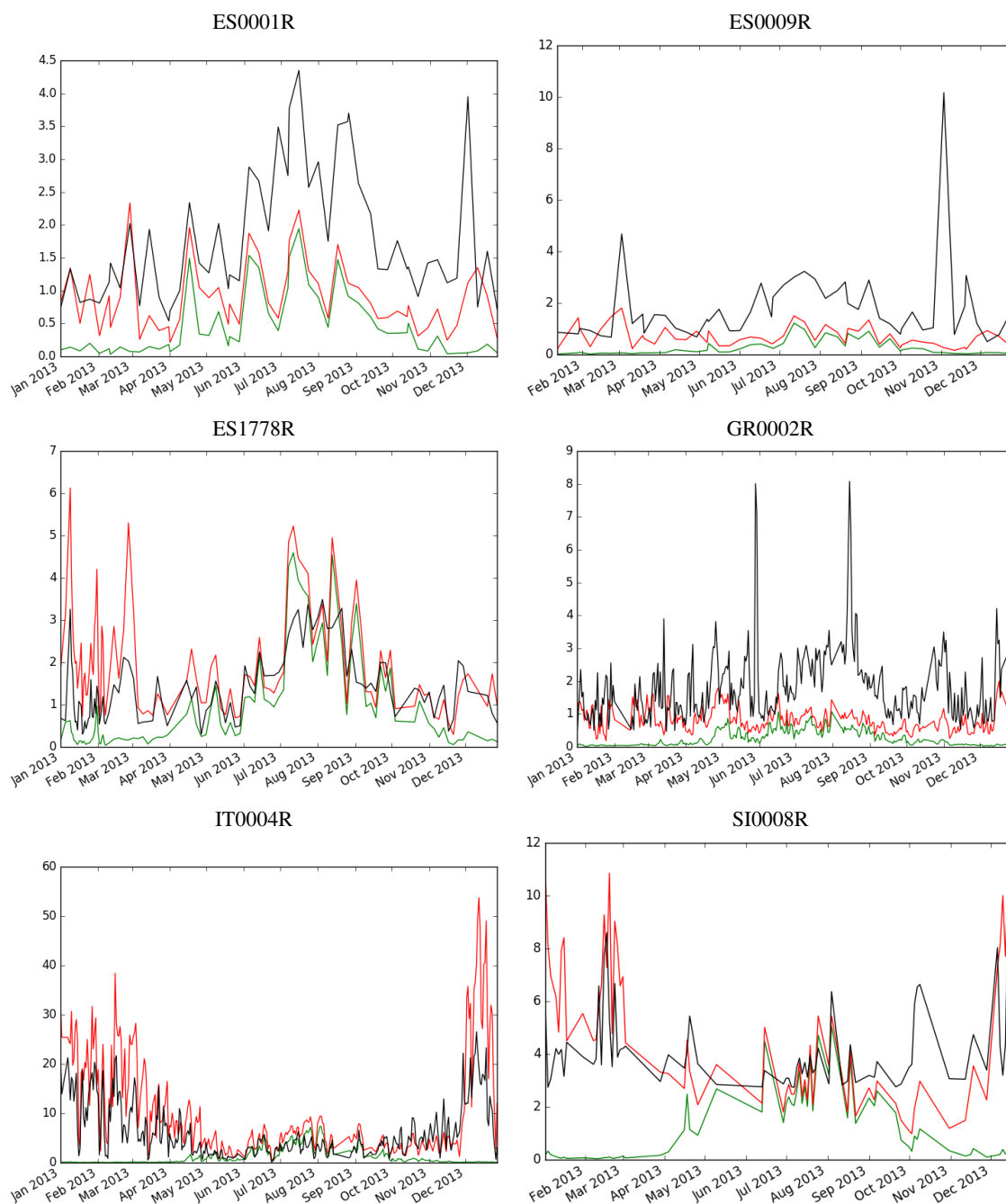
Figure 12. Temporal evolution of modeled (red line) and measured (black line) OC concentrations (in in μg m^{-3}) for stations in the South of Europe. The green line corresponds to Organic Carbon from biogenic compounds.

Geoscientific
Model Development
Discussions
Open Access

Figure 13. Temporal evolution of modeled (red line) and measured (black line) Organic Carbon concentrations (in in μg m^{-3}) for stations in the South of Europe. The green line corresponds to OC from biogenic compounds.
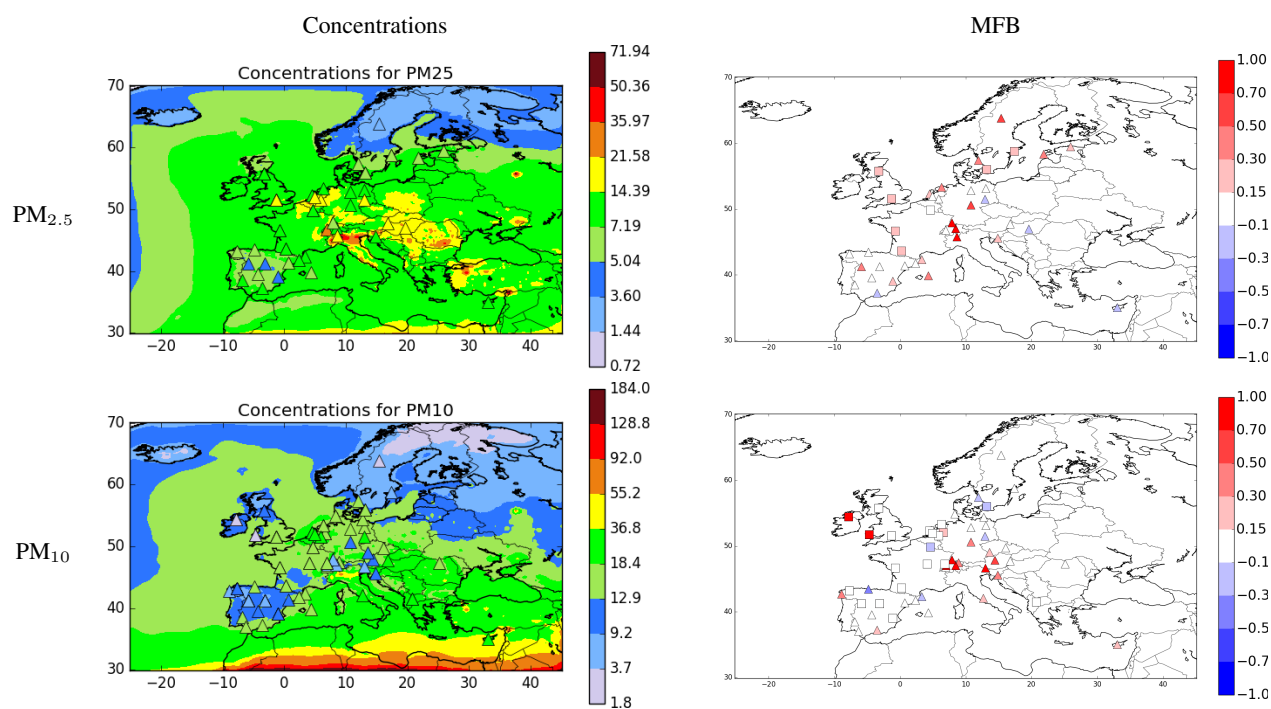
Figure 14. Modeled concentrations (in in μg m^{-3}) and MFB for PM2.5 and PM$_{10}$ in 2013. Triangles correspond to measured concentrations in the left and to the MFB value in the right.
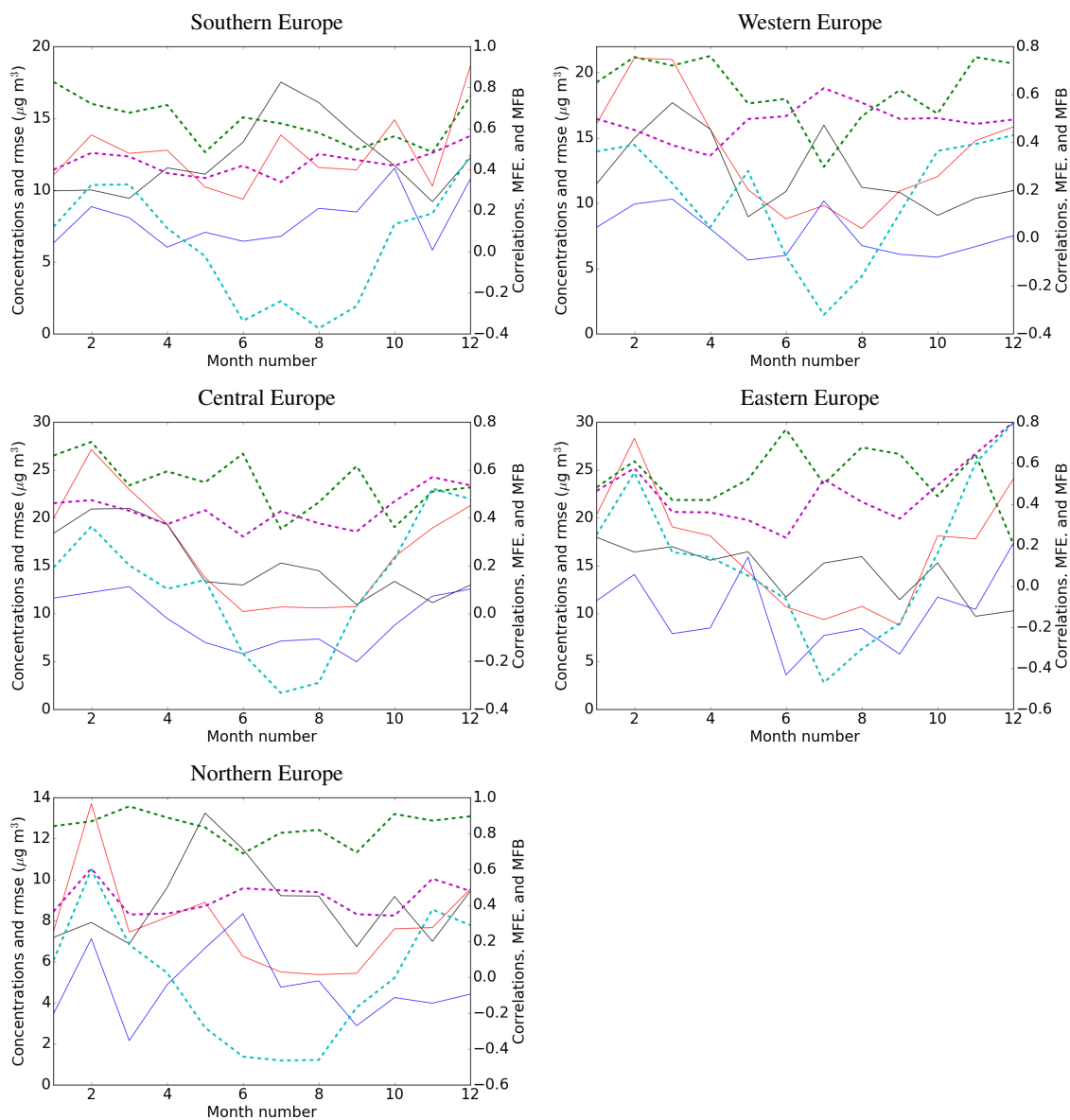
Figure 15. Seasonal evolution of statistics by regions for PM$_{2.5}$: Monthly mean measured concentrations (black), monthly mean modeled concentrations (red), monthly RMSE (blue), monthly spatiotemporal correlations (green), monyhly MFB (cyan) and monthly MFE (magenta). Solid curves refer to the left axis while dotted curves refer to the right axis.

Figure 16. QQ scatter plot of PM_{10} and of $PM_{2.5}$ (bottom right panel) modeling results against measurements for the several regions. SE: Southern Europe. WE: Western Europe. CE: Central Europe. EE: Eastern Europe. NE: Northern Europe.

Figure 17. Seasonal evolution of statistics by regions for PM_{10}: Monthly mean measured concentrations (black), monthly mean modeled concentrations (red), monthly RMSE (blue), monthly spatiotemporal correlations (green), monyhly MFB (cyan) and monthly MFE (magenta). Solid curves refer to the left axis while dotted curves refer to the right axis.
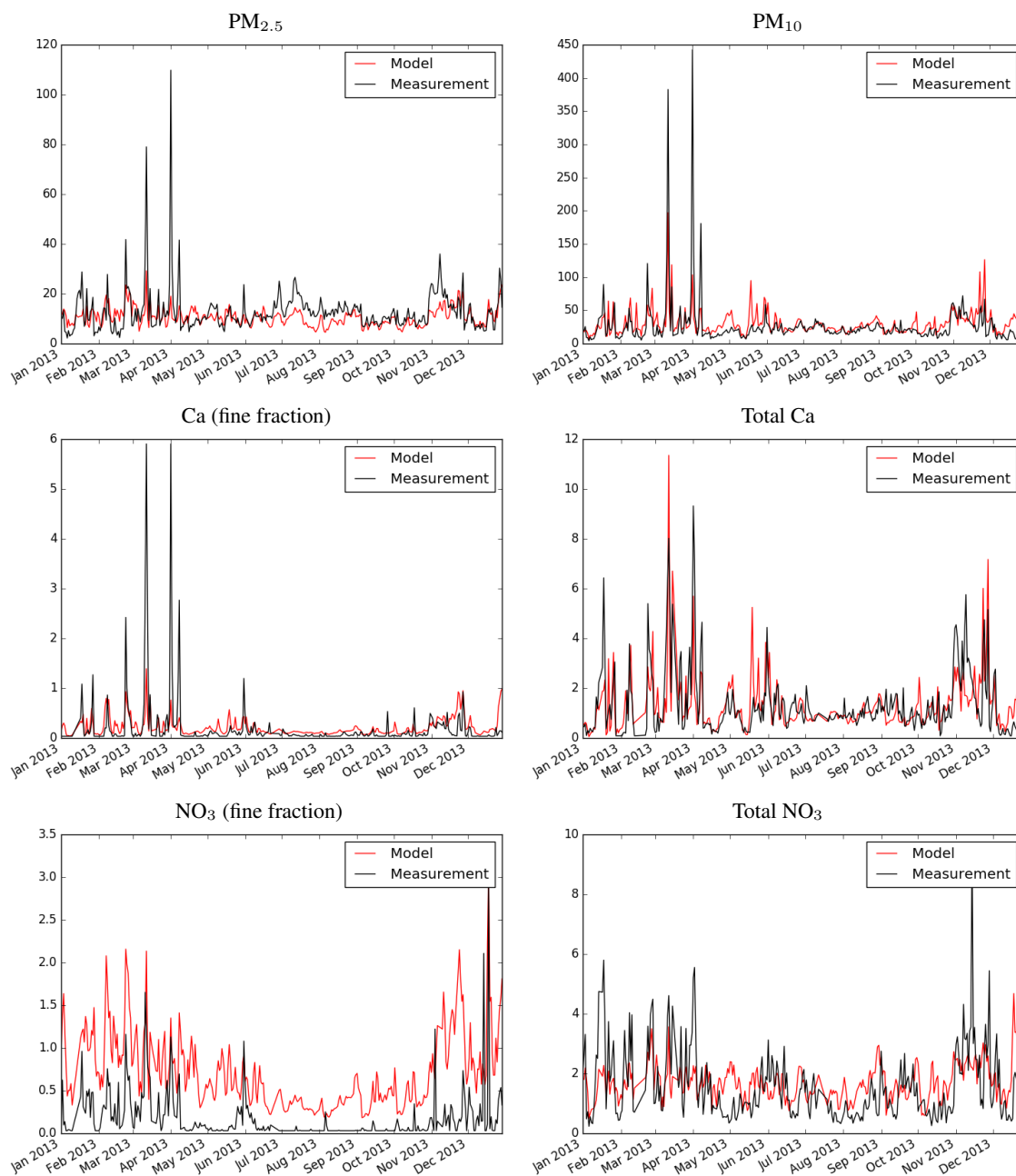
Figure 18. Modeled (red) and measured (black) concentrations of $PM_{2.5}$, PM_{10}, Ca (fine fraction and total) and NO_3 (fine fraction and total) in $\mu g\ m^{-3}$ for the Cyprus station CY0002R.
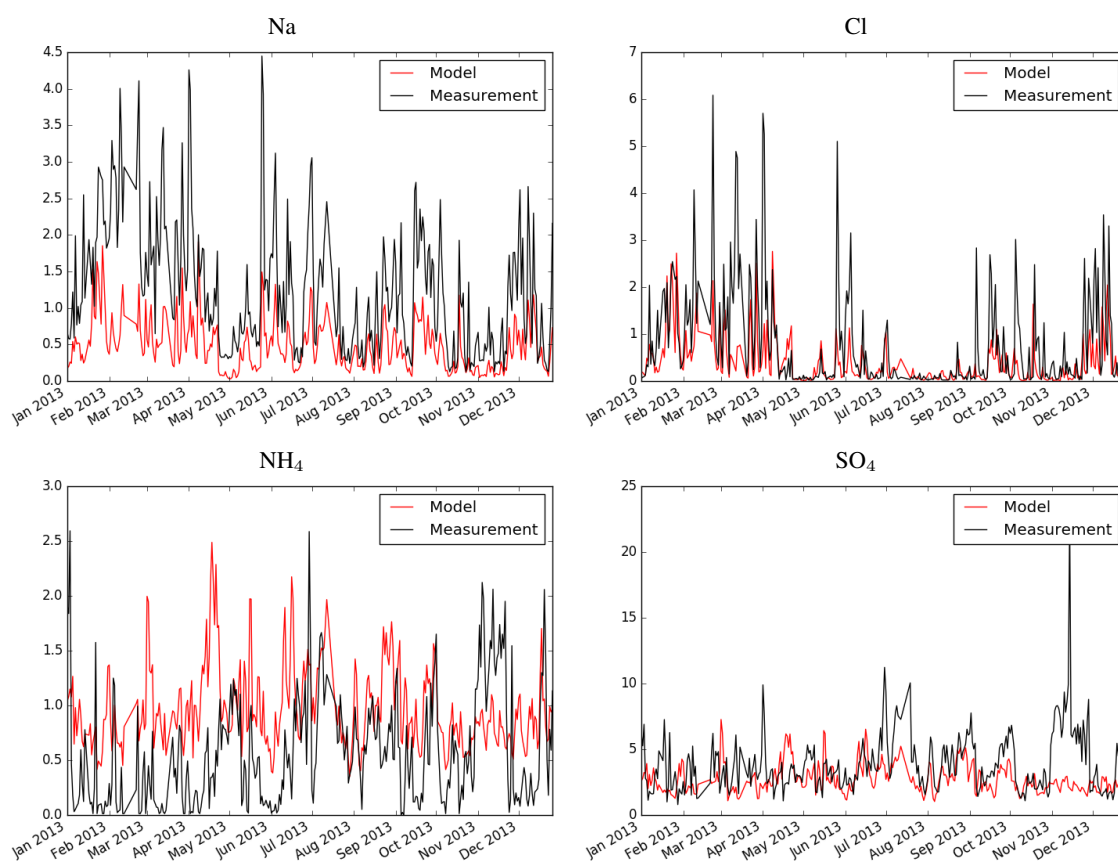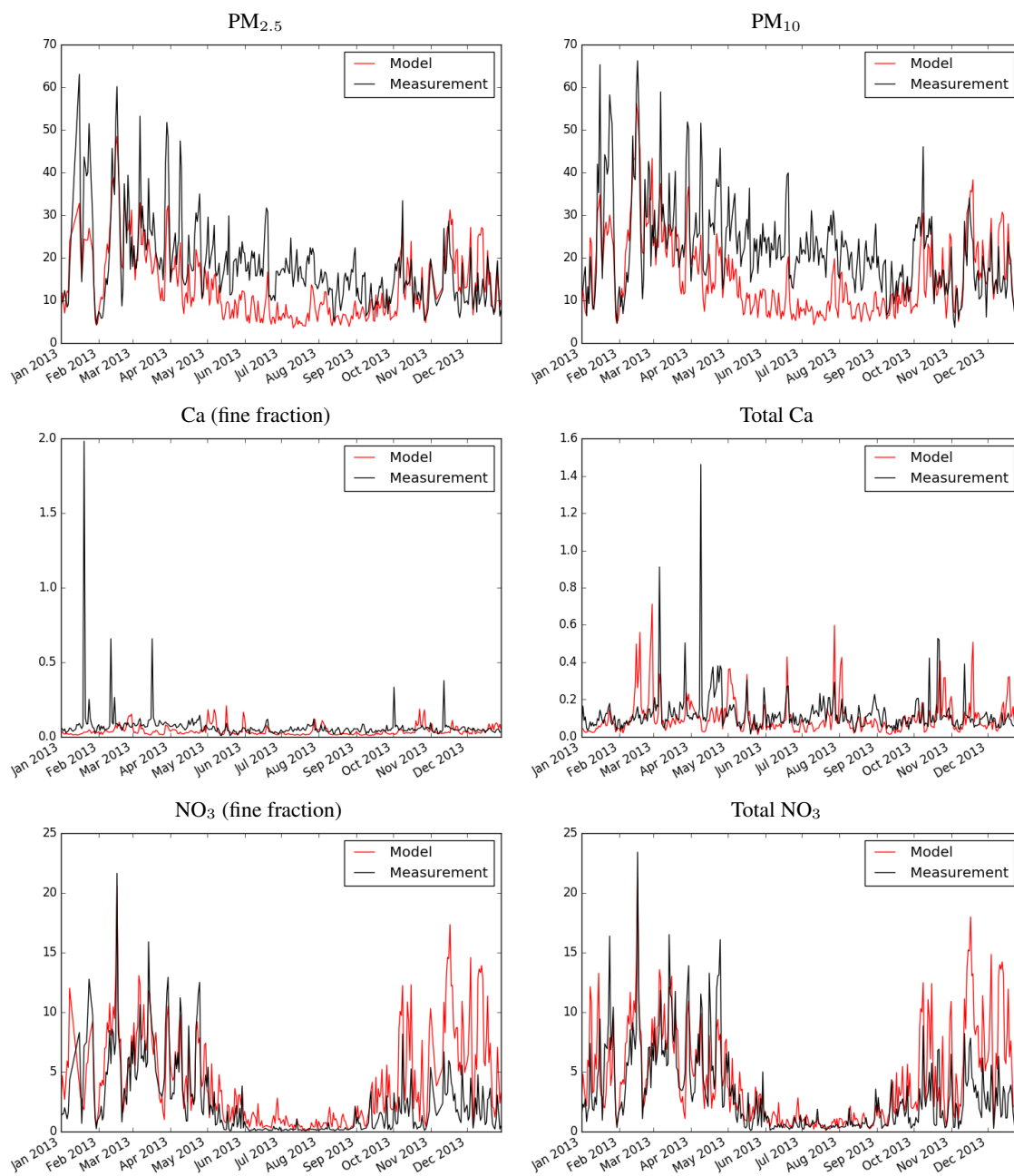
Figure 19. Modeled (red) and measured (black) concentrations of Na, Cl, NH_4, SO_4 in μg m^{-3} for the Cyprus station CY0002R.

Figure 20. Modeled (red) and measured (black) concentrations of $PM_{2.5}$, PM_{10}, Ca (fine fraction and total) and NO_3 (fine fraction and total) in $\mu g\ m^{-3}$ for the station DE0044R (Germany)
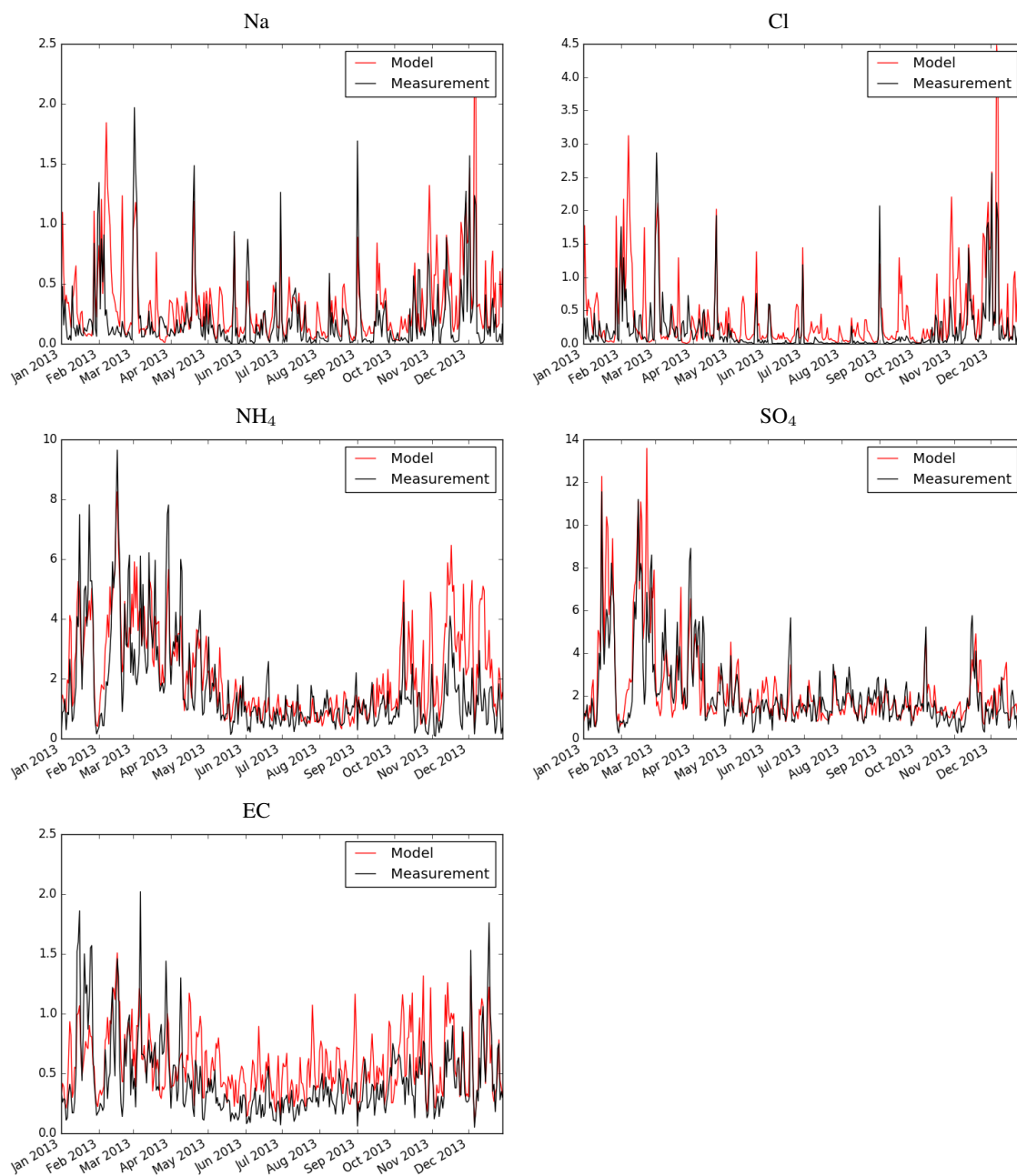
Figure 21. Modeled (red) and measured (black) concentrations of Na, Cl, NH_4, SO_4, EC in μg m^{-3} for the station DE0044R (Germany).